Jefferson.

Thomas Jefferson University
Jefferson Digital Commons

Department of Neuroscience | Sidney Kimmel Medical College

8-23-2017

Calcineurin Dysregulation Underlies Spinal Cord Injury-Induced K(+) Channel Dysfunction in DRG Neurons.

Benjamin M. Zemel
Thomas Jefferson University, Benjamin.Zemel@jefferson.edu

Tanziyah Muqeem
Thomas Jefferson University, tanziyah.muqeem@jefferson.edu

Eric V. Brown
Thomas Jefferson University, eric.v.brown@jefferson.edu

Miguel Goulão
Thomas Jefferson University; University of Minho, miguel.gmiguel.goulaodacunha@jefferson.edu

Mark W Urban
Thomas Jefferson University, mark.urban@jefferson.edu

See next page for additional authors

Let us know how access to this document benefits you

Follow this and additional works at: http://jdc.jefferson.edu/department_neuroscience

Part of the Neurosciences Commons

Recommended Citation
Zemel, Benjamin M.; Muqeem, Tanziyah; Brown, Eric V.; Goulão, Miguel; Urban, Mark W; Tymanskyj, Stephen R.; Lepore, Angelo C.; and Covarrubias, Manuel, "Calcineurin Dysregulation Underlies Spinal Cord Injury-Induced K(+) Channel Dysfunction in DRG Neurons." (2017). *Department of Neuroscience.* Paper 29.
http://jdc.jefferson.edu/department_neuroscience/29

This Article is brought to you for free and open access by the Jefferson Digital Commons. The Jefferson Digital Commons is a service of Thomas Jefferson University's Center for Teaching and Learning (CTL). The Commons is a showcase for Jefferson books and journals, peer-reviewed scholarly publications, unique historical collections from the University archives, and teaching tools. The Jefferson Digital Commons allows researchers and interested readers anywhere in the world to learn about and keep up to date with Jefferson scholarship. This article has been accepted for inclusion in Department of Neuroscience by an authorized administrator of the Jefferson Digital Commons. For more information, please contact: JeffersonDigitalCommons@jefferson.edu.

Authors
Benjamin M. Zemel, Tanziyah Muqeem, Eric V. Brown, Miguel Goulão, Mark W Urban, Stephen R. Tymanskyj, Angelo C. Lepore, and Manuel Covarrubias

This article is available at Jefferson Digital Commons: http://jdc.jefferson.edu/department_neuroscience/29

Cellular/Molecular

Calcineurin Dysregulation Underlies Spinal Cord Injury-Induced K^+ Channel Dysfunction in DRG Neurons

Benjamin M. Zemel,[1,2] Tanziyah Muqeem,[1,2] Eric V. Brown,[1,2] Miguel Goulão,[1,3,4] Mark W. Urban,[1,2] Stephen R. Tymanskyj,[1] Angelo C. Lepore,[1,2] and Manuel Covarrubias[1,2]

[1]Department of Neuroscience and Vickie and Jack Farber Institute for Neuroscience, Sidney Kimmel Medical College, and [2]Jefferson College of Biomedical Sciences, Thomas Jefferson University, Philadelphia, Pennsylvania 19107, [3]Life and Health Sciences Research Institute, School of Medicine, University of Minho, Campus de Gualtar, 4710-057 Braga, Portugal, and [4]Life and Health Sciences Research Institute (ICVS)/3B's PT Government Associate Laboratory, 4710-057 Braga/Guimarães, Portugal

Dysfunction of the fast-inactivating Kv3.4 potassium current in dorsal root ganglion (DRG) neurons contributes to the hyperexcitability associated with persistent pain induced by spinal cord injury (SCI). However, the underlying mechanism is not known. In light of our previous work demonstrating modulation of the Kv3.4 channel by phosphorylation, we investigated the role of the phosphatase calcineurin (CaN) using electrophysiological, molecular, and imaging approaches in adult female Sprague Dawley rats. Pharmacological inhibition of CaN in small-diameter DRG neurons slowed repolarization of the somatic action potential (AP) and attenuated the Kv3.4 current. Attenuated Kv3.4 currents also exhibited slowed inactivation. We observed similar effects on the recombinant Kv3.4 channel heterologously expressed in Chinese hamster ovary cells, supporting our findings in DRG neurons. Elucidating the molecular basis of these effects, mutation of four previously characterized serines within the Kv3.4 N-terminal inactivation domain eliminated the effects of CaN inhibition on the Kv3.4 current. SCI similarly induced concurrent Kv3.4 current attenuation and slowing of inactivation. Although there was little change in CaN expression and localization after injury, SCI induced upregulation of the native regulator of CaN 1 (RCAN1) in the DRG at the transcript and protein levels. Consistent with CaN inhibition resulting from RCAN1 upregulation, overexpression of RCAN1 in naive DRG neurons recapitulated the effects of pharmacological CaN inhibition on the Kv3.4 current and the AP. Overall, these results demonstrate a novel regulatory pathway that links CaN, RCAN1, and Kv3.4 in DRG neurons. Dysregulation of this pathway might underlie a peripheral mechanism of pain sensitization induced by SCI.

Key words: calcineurin; Kv3.4; pain; RCAN1; spinal cord injury

Significance Statement

Pain sensitization associated with spinal cord injury (SCI) involves poorly understood maladaptive modulation of neuronal excitability. Although central mechanisms have received significant attention, recent studies have identified peripheral nerve hyperexcitability as a driver of persistent pain signaling after SCI. However, the ion channels and signaling molecules responsible for this change in primary sensory neuron excitability are still not well defined. To address this problem, this study used complementary electrophysiological and molecular methods to determine how Kv3.4, a voltage-gated K^+ channel robustly expressed in dorsal root ganglion neurons, becomes dysfunctional upon calcineurin (CaN) inhibition. The results strongly suggest that CaN inhibition underlies SCI-induced dysfunction of Kv3.4 and the associated excitability changes through upregulation of the native regulator of CaN 1 (RCAN1).

Introduction

Accumulating evidence suggests that changes in the peripheral nervous system play a major role in promoting pain sensitization after spinal cord injury (SCI) (Bedi et al., 2010; Yang et al., 2014). In neuropathic pain, ion channel dysfunction is associated with

Received Feb. 15, 2017; revised July 14, 2017; accepted July 19, 2017.

Author contributions: B.M.Z., A.C.L., and M.C. designed research; B.M.Z., T.M., E.V.B., M.G., M.W.U., and S.R.T. performed research; B.M.Z., T.M., and E.V.B. analyzed data; B.M.Z. and M.C. wrote the paper.

This work was supported by the Vickie and Jack Farber Family Foundation (M.C.), the Dean's Transformational Science Award (M.C.), and the National Institutes of Health (Grant NS090689 to B.M.Z. and Grant NS079855 to M.C.). This work is part of the requirements toward a doctoral degree in neuroscience from Thomas Jefferson University for B.M.Z. We thank Dr. Rejji Kuruvilla (Johns Hopkins University) for sharing the anti-RCAN1 antibody; Drs. Jeffrey Benovic, Masumi Eto, and Bernardo Rudy for experimental suggestions and helpful feedback; Drs. David Ritter and Matthew Dalva for helpful comments on an earlier version of this manuscript; Dr. Le Ma for assistance with embryonic cultures; and Dr. Maria Yolanda Covarrubias for help with confocal microscopy.

The authors declare no competing financial interests.

Correspondence should be addressed to Manuel Covarrubias, M.D., Ph.D., Department of Neuroscience and Vickie and Jack Farber Institute for Neuroscience, Sidney Kimmel Medical College, Thomas Jefferson University, 233 South 10th Street, BLSB 231, Philadelphia, PA 19107. E-mail: Manuel.Covarrubias@jefferson.edu.

hyperexcitability in dorsal root ganglion (DRG) neurons (Dubin and Patapoutian, 2010; Gold and Gebhart, 2010; Hughes et al., 2012; Trimmer, 2014; Tsantoulas and McMahon, 2014; Walters, 2015). Whether analogous changes mediate SCI-induced pain sensitization, which does not involve direct injury of primary sensory neurons, remains to be determined. Here, we elucidated a novel mechanism involving dysfunction of the Kv3.4 channel induced by dysregulation of calcineurin (CaN) in DRG neurons after SCI.

Homotetrameric Kv3.4 channels are highly expressed and are major regulators of action potential (AP) repolarization in small-diameter DRG neurons. Kv3.4 channel dysfunction in DRG neurons has been implicated in chronic pain syndromes (Chien et al., 2007; Duan et al., 2012; Li et al., 2014; Ritter et al., 2015a). Protein kinase C (PKC) modulates Kv3.4 by phosphorylating four serines within the N-terminal inactivation domain (NTID) (Covarrubias et al., 1994; Beck et al., 1998; Antz et al., 1999). This post-translational modification quickly switches the Kv3.4 current phenotype from fast-inactivating to slow/non-inactivating. However, the phosphatase that reverses it was not known. SCI induces attenuation of the Kv3.4 current and slowing of inactivation (Ritter et al., 2012; Ritter et al., 2015a). This suggests a homeostatic mechanism whereby slower inactivation strengthens the remaining Kv3.4 current as it strives to oppose SCI-induced hyperexcitability. In support of a dysregulated physiological role, severe siRNA-induced Kv3.4 knock-down in DRG neurons broadens the AP and eliminates acceleration of AP repolarization upon PKC activation (Ritter et al., 2012). To investigate molecules responsible for SCI-induced attenuation of the Kv3.4 current, we hypothesize that calcineurin (CaN) modulates Kv3.4 function. SCI-induced dysregulation of CaN would impair Kv3.4 function, promoting DRG hyperexcitability and the associated pain sensitization.

CaN is a Ca^{2+}-dependent serine-threonine protein phosphatase expressed in the nervous system, including the DRG (Goto et al., 1986; Strack et al., 1996). The immunosuppressants tacrolimus (FK506) and cyclosporin A (CsA) are CaN inhibitors responsible for CaN inhibitor-induced pain syndrome (CIPS) in subsets of transplant patients (Grotz et al., 2001; Fujii et al., 2006; Noda et al., 2008; Prommer, 2012; Azzi et al., 2013). Other studies found downregulation of CaN in the dorsal horn after rat sciatic nerve ligation (Miletic et al., 2002; Miletic et al., 2011; Miletic et al., 2013; Miletic et al., 2015). Intrathecal injection of CaN protein was sufficient to attenuate the resulting hyperalgesia (Miletic et al., 2013). Although these studies link reduced CaN activity and persistent pain syndromes, the downstream ion channel targets responsible for the underlying hyperexcitability are not known. A recent study reported upregulation of the endogenous regulator of CaN 1 (RCAN1) in rat spinal cord after SCI (Wang et al., 2016). RCAN1 upregulation typically inhibits CaN, which might affect CaN-dependent modulation of ion channels in DRG neurons (Davies et al., 2007; Liu et al., 2009; Li et al., 2011; Patel et al., 2015). However, until recently, there was no evidence for such a maladaptive change in the DRG.

In this study, we found that CaN inhibition prolonged the AP of small-diameter DRG neurons, which is associated with attenuation of the Kv3.4 current. Concomitantly, CaN inhibition slowed Kv3.4 fast inactivation. SCI induced changes in the Kv3.4 current of small-diameter DRG neurons that resemble those induced by CaN inhibition. Elucidating a mechanism, first, we found that modulation of Kv3.4 by CaN depends on four serines within the NTID of Kv3.4. Therefore, CaN is a phosphatase that counteracts PKC action on the NTID. Second, we determined that RCAN1 is upregulated in the DRG after SCI and that overexpression of RCAN1 in naive DRG neurons recapitulates the effects of CaN inhibition on the Kv3.4 current and the AP. We propose a pathway that links CaN and RCAN1 to functional modulation of the Kv3.4 channel in DRG neurons. Dysregulation of this pathway after SCI could be a major factor contributing to the peripheral hyperexcitability associated with SCI-induced persistent pain.

Materials and Methods

DRG dissociation. DRG neurons were harvested and dissociated from adult female Sprague Dawley rats (Taconic) as described previously (Ritter et al., 2012). After removal of the spinal cord, the cervical DRGs C3–C7 were harvested. Nerve fibers coming from the DRGs were trimmed and ganglia placed in Hank's buffered saline solution (HBSS) + 10 mM HEPES. DRGs were then treated with collagenase (1.5 mg/ml in HBSS + 10 mM HEPES solution) for 30 min at 37°C, followed by 2 washes with HBSS + 10 mM HEPES. This was followed by an incubation with trypsin (1.0 mg/ml in HBSS + 10 mM HEPES) for 30 min at 37°C. DRGs were then placed in L-15 Leibovitz medium supplemented with 10% fetal bovine serum, 38 mM glucose, 2 mM L-glutamine, 24 mM $NaHCO_3$, and 2% penicillin–streptomycin and mechanically dissociated with a fire polished Pasteur pipette. Dissociated DRG neurons were plated on glass polyornithine-coated coverslips, incubated at 37°C, and used for electrophysiological experiments within 2–3 h after harvesting.

For embryonic cultures, DRGs were dissected out from embryonic day 18 (E18) rat embryos, washed once in HBSS, and incubated at 37°C with 0.25% trypsin for 10–15 min. Trypsin-treated DRGs were resuspended in L15 medium plus 10% horse serum and then mechanically triturated with a fire-polished glass pipette. Dissociated rat DRG neurons ($\sim 7.5 \times 10^5$ cells) were transfected with various constructs by nucleofection (Lonza) using reagent P3 and the CU-133 program and then sets of ~30,000 cells were cultured on 18 mm glass coverslips coated with 10 μg/ml poly-D-lysine and 10 μg/ml laminin in F12 medium (with the N3 supplement, 40 mM glucose, and 25 ng/ml NGF).

Heterologous expression in mammalian cells. Chinese hamster ovary (CHO) cells were grown on 10 cm tissue culture dishes in F12 medium containing a 2 mM L-glutamine, 10% heat-inactivated fetal bovine serum, and 0.1% penicillin–streptomycin. Cells were kept in a humidified incubator at 37°C (5% CO_2) and passaged every ~4 d. After ~30 passages, cells were discarded. For heterologous expression, cells were cotransfected with Kv3.4 and enhanced green fluorescent protein (EGFP) cDNAs using Lipofectamine 2000 (Thermo Fisher Scientific) according to the manufacturer's instructions. Transfections were performed in 35 mm dishes and then plated onto 5 mm glass coverslips coated with polyornithine. Under epifluorescence conditions, EGFP expression allowed identification of successfully transfected cells.

Transfection and staining of acutely dissociated DRG neurons. DRG neurons were isolated and plated as described above. Two hours after plating on glass coverslips in a 35 mm dish, cells were transfected with RCAN1-Flag (gift from Jeffery Molkentin, University of Cincinnati; Addgene plasmid # 65413) and EGFP plasmids or with an EGFP plasmid alone. Transfections were done using Qiagen's Effectene transfection reagent following the instructions provided by the manufacturer. Briefly, 150 μl of EC buffer was combined with 1 μg of DNA (1 μg of EGFP vs 0.75 μg of RCAN1-Flag + 0.25 μg of EGFP) and 8 μl of the enhancer reagent. After a 5 min incubation, 25 μl of Tranfectene reagent was added. Subsequently (10 min later), this solution was added to DRG neurons, which were then incubated at 37°C for 4–6 h. The medium was then swapped out and replaced every 5–15 h until DRGs were recorded 36–48 h after transfection. Cells not used for electrophysiology were fixed with 4% PFA for 10 min and proceeded to be blocked with PBS containing 0.2% Triton X-100 and 10% goat serum for 1 h at room temperature. Coverslips were then stained overnight at 4°C in PBS containing 0.1% Tween, 2% goat serum, and rabbit anti-Flag antibodies 1:1000 (Abcam catalog #ab1162 RRID:AB_298215). Coverslips were then washed with PBS and a coverslip was mounted on a slide using DAPI Prolong Gold Antifade Reagent.

DOI:10.1523/JNEUROSCI.0434-17.201710.1523/JNEUROSCI.0434-17.2017
Copyright © 2017 the authors 0270-6474/17/378257-17$15.00/0

Table 1. Passive and active properties of APs and effects of calcineurin inhibition

	DMSO (vehicle)		FK506		CaN inhibitory peptide	
	Before	5 min	Before	5 min	10 min	Last
RMP (mV)	−57.3 ± 1.8	−63.6 ± 2.1***	−63.7 ± 2.0	−63.4 ± 2.0	−66.3 ± 2.3	−64.5 ± 3.1
Input resistance (GΩ)	0.8 ± 0.1	1 ± 0.2	0.9 ± 0.1	0.9 ± 0.2	0.9 ± 0.2	0.7 ± 0.1
Capacitance (pF)	14.2 ± 0.7	—	15.1 ± 0.8	—	15.9 ± 1.0	—
Diameter (μm)	20.8 ± 0.7	—	21.4 ± 0.6	—	23.3 ± 1.0	—
Threshold (mV)	−35.6 ± 1.4	−38.6 ± 1.5*	−37.0 ± 1.5	−36.4 ± 2.0	−34.5 ± 3.7	−31.3 ± 3.6
Amplitude (mV)	109.6 ± 3.0	112.0 ± 2.7	114.0 ± 2.7	107.3 ± 4.0**	113.3 ± 5.2	107.4 ± 7.7
AHP (mV)	−72.2 ± 1.1	−75.8 ± 1.3***	−75.5 ± 1.0	−76.5 ± 1.2	−74.9 ± 2.4	−70.1 ± 2.6*
APD_{90} (ms)	1.06 ± 0.09	0.96 ± 0.07	0.88 ± 0.06	1.12 ± 0.11**	0.91 ± 0.05	1.28 ± 0.12**
Max depolarization rate (mV/ms)	85.0 ± 11.0	94.5 ± 12.4	103.0 ± 11.3	75.1 ± 10.5***	107.7 ± 10.5	86.5 ± 13.4**
Max repolarization rate (mV/ms)	43.3 ± 4.5	46.6 ± 5.2	45.5 ± 3.0	35.2 ± 3.1****	43.2 ± 3.2	30.5 ± 3.2***
n	14		15		6	

Shown are changes in DRG AP properties as a result of calcineurin inhibition. The 5 min time point for DMSO and FK506 experiments is 5 min after wash-in. The last time point for CaN inhibitory peptide experiments ranged from 15–30 min. Student's *t* test used for comparisons of paired data.

RMP, Resting membrane potential; AHP, afterhyperpolarization.

*$p \leq 0.05$, **$p \leq 0.01$, ***$p \leq 0.001$, ****$p \leq 0.0001$.

Electrophysiological recordings. As reported previously, all electrophysiological experiments with acutely dissociated DRG neurons were performed at room temperature (20–24°C) (Ritter et al., 2012). A PIP5 micropipette puller (HEKA Instruments) was used to pull patch electrodes made from borosilicate thin-walled patch glass (Warner Instrument). Electrodes tip resistances ranged between 1 and 3 MΩ after fire polishing. The Multiclamp 700B amplifier (Molecular Devices) was used to amplify signals and a computer running Clampex 10.5 (Molecular Devices) was used for data acquisition and storage. Signals were low-pass filtered at 2 kHz (Multiclamp internal 4-pole Bessel filter) and digitized at 10 kHz (Digidata 1440; Molecular Devices). In cell-attached macropatch experiments, the bath and pipette solution contained the following (in mM): 130 choline-Cl, 5 KCl, 1 $MgCl_2$, 2 $CaCl_2$, 10 HEPES, and 50 sucrose, pH 7.4 adjusted with choline base. The membrane potential in the cell-attached configuration was estimated from the following relation: $V_m = V_C + V_R$, where V_C is the command voltage and V_R is the resting membrane potential of the neurons. The V_R in this study was −60.6 ± 1.5 mV ($n = 29$ neurons), which closely replicates previously published measurements (Ritter et al., 2012, 2015a). For whole-cell current-clamping experiments, the bath solution contained the following (in mM): 130 NaCl, 5 KCl, 2 $CaCl_2$, 1 $MgCl_2$, and 10 HEPES, pH 7.4. The pipette solution contained the following (in mM): 130 K-MES, 1 $CaCl_2$, 1 EGTA, 10 HEPES, 2 Mg-ATP, and 0.3 Tris-GTP, pH 7.3. Liquid junction potentials in cell-attached macropatch experiments (0 mV) and current-clamp recordings (+15.5 mV) were calculated using Clampex version 10.5 software and were corrected offline.

Once the whole-cell configuration was obtained, the passive properties of the cell were determined (Table 1) and AP recordings in the absence and presence of inhibitors typically began 5–10 min after establishing the whole-cell configuration. Input resistance, series resistance, and resting membrane potential were monitored during the recordings. Series resistance was typically ≤7 MΩ, of which 70% was compensated. Somatic APs were elicited using a brief 0.5 ms current injection stimulus. Bridge balance compensation was used throughout all experiments.

Phase-plane plots were used to determined AP threshold (where the plot deviates from 0 mV/ms) and the maximum rates of depolarization and repolarization. The AP amplitude was measured as the difference between the peak overshoot and the afterhyperpolarization. The width of the AP at 90% of the AP amplitude (APD_{90}) was measured as described previously (Ritter et al., 2012). The APD_{90} was used to avoid artifacts resulting from AP waveform variations, which have greater influence on the APD_{50} (AP width at 50% of the AP amplitude).

Electrophysiological experiments on CHO cells were conducted using the instrumentation described above. In cell-attached macropatch experiments, the bath contained the following (in mM): 150 KCl, 10 HEPES, 1.5 $CaCl_2$, and 1 $MgCl_2$, pH 7.4 with KOH. This external solution nullifies the resting membrane potential of the cell ($V_m \approx V_C$). The pipette solution contained the following (in mM): 150 NaCl, 10 HEPES, 2 KCl, 1.5 $CaCl_2$, and 1 $MgCl_2$, pH7.4 with NaOH.

Analysis of electrophysiological experiments. Clampfit version 10.5 (Molecular Devices) and OriginPro version 9.1 (Origin Laboratory) were used for data processing and analysis. The peak chord conductance (G_p) in cell-attached patches was calculated using the following relation:

$$G_p = I_p/(V_m - V_{rev}),$$

where I_p is the peak current, V_m is the membrane potential estimated as stated above, and $V_{rev} = -73$ mV, as estimated previously (Ritter et al., 2012). To normalize the peak chord conductance (G_p), the maximum peak chord conductance (G_{pmax}) was calculated from the following best-fit fourth-order Boltzmann function:

$$G_p(V_m) = \{G_{pmax}/[1 + \exp((V_s - V_m)/k)]\}^4,$$

where V_s is the activation midpoint voltage of a single subunit and k is the slope factor. The midpoint voltage ($V_{1/2}$) of the G_p/V_m curve was calculated from the following equation:

$$V_{1/2} = V_s + 1.67k$$

The steady-state inactivation parameters were determined from the best-fit to the following simple Boltzmann function:

$$I_p(V_m) = I_{pmax}/[1 + \exp((V_m - V_{1/2})/k)],$$

where $V_{1/2}$ is the midpoint voltage of the curve and k is the slope factor. In some instances, the sum of two Boltzmann terms yielded a better bit. Therefore, the median voltage was used to describe the midpoint position of the double Boltzmann curve along the voltage axis.

Reagents. FK506, CsA, and the CaN auto-inhibitory peptide were purchased from Tocris Biosciences. Stock solutions of FK506 and CsA stocks were made in dimethyl sulfoxide (DMSO) with the final concentrations in the recording solution of 0.5–2%; the CaN auto-inhibitory peptide stocks were made in nuclease-free H_2O. The rat Kv3.4 plasmid used for CHO cell transfection was a gift from Olaf Pongs (University of Hamburg, Germany).

Animals and SCI model. Adult female Sprague Dawley rats (200–250 g) were purchased from Taconic Farms and treated according to a protocol approved by the Thomas Jefferson University Institutional Animal Care and Use Committee. SCI and laminectomy surgeries were performed as described previously (Nicaise et al., 2012). Animals were anesthetized using a mixture of ketamine (95 mg/kg), xylazine (10 mg/kg), and acepromazine (0.075 mg/kg). A small incision was made in the skin overlying cervical levels C3–C7. The overlying musculature was incised and reflected and a laminectomy performed at C5. For SCI, the animal was then stabilized with two forceps clamping the C2 and C7 vertebral processes and placed in the Infinite Horizons Impactor (Precision Systems and Instrumentation). A 1 mm impactor tip was centered over the exposed right side of the spinal cord, raised to height of 4 mm, and a 200 kilodyne unilateral contusion delivered (range, 195–205 kilodynes). The

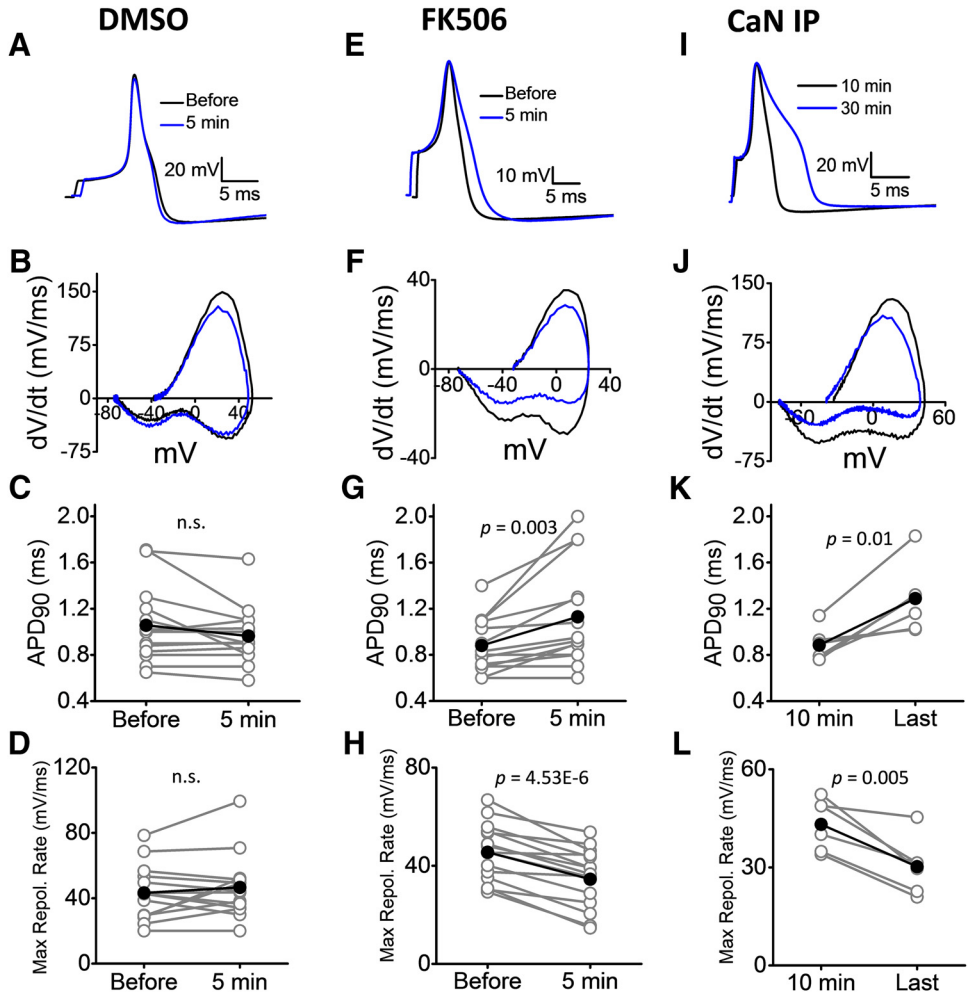

Figure 1. CaN inhibition alters the AP waveform in DRG neurons. ***A***, APs before and after exposure to DMSO (left). ***B***, Phase plane plots of the waveforms represented in (***A***). ***C***, Comparison of the APD_{90} before and after a 5 min exposure to DMSO ($n = 14$; DF = 13; $t_{stat} = 1.93$). ***D***, Comparison of the maximum repolarization rate (Max. repol.) before and after a 5 min exposure to DMSO ($n = 14$; DF = 13; $t_{stat} = 1.11$). ***E–H***, Same as ***A–D*** except for the exposure to 10 μM FK506 ($n = 15$; DF(APD_{90}) = 14; t_{stat}(APD_{90}) = 3.51; DF(Max. repol.) = 14; t_{stat} (Max. repol.) = 7.21). ***I–L***, Same as ***A–D*** except for the exposure to 50 μM intracellular CaN inhibitory peptide ($n = 6$ for ***K*** and $n = 6$ for ***L***); DF(APD_{90}) = 5; t_{stat}(APD_{90}) = 3.97; DF(Max. repol.) = 5; t_{stat} (Max. repol.) = 4.75). *p*-values are indicated in the graphs (Student's paired *t* test).

muscle and skin were closed in layers and animals were allowed to recover for 2 weeks. Laminectomy controls received all procedures except a contusion. Two weeks after injury, animals were killed by overdose of ketamine (380 mg/kg), xylazine (40 mg/kg), acepromazine (0.3 mg/kg), followed by thoracotomy. The spinal column was then extracted and C3–C7 DRG neurons ipsilateral to the SCI were extracted and subjected to the same dissociation protocol described above.

RNA FISH. Rats that had received either SCI or laminectomy underwent a thoracotomy followed by cardiac perfusion with 4% paraformaldehyde. C4–C6 DRGs ipsilateral to the injury were then removed and sectioned at 30 μm on a cryostat before being mounted on glass slides. Sections were then stained with Quasar 570 tagged antisense oligonucleotides against rat RCAN1 mRNA. All reagents used for this procedure, including antisense probes, were obtained commercially (Custom Stellaris FISH, Biosearch Technologies). The simultaneous FISH (antisense RCAN1 probes) and immunofluorescence (anti-pan-cadherin antibodies) protocol used for the staining procedure was performed according to the manufacturer's instructions.

DAPI with Prolong Gold Antifade Reagent was used after the secondary antibody incubation, eliminating the need for sealing coverslips with clear nail polish. *Z*-stacks were obtained using a Nikon C1 Plus confocal microscope at the Bioimaging Facility of the Sidney Kimmel Cancer Center (NIH Cancer Center Core Grant 5 P30 CA-56036) and images precisely ½ way through each section were taken and analyzed using ImageJ. Puncta were counted within the bounds of individual neurons as shown by pan-cadherin staining.

Immunofluorescence studies. Animals were killed 2 weeks after surgery and transcardially perfused with 0.9% saline followed by 4% paraformaldehyde. DRGs from C4–C6 ipsilateral to the unilateral spinal contusion were harvested and stored in 4% paraformaldehyde (24 h), followed by 0.1 M phosphate buffer (24 h), and finally in 30% sucrose containing phosphate buffer (3 d). The tissue was then embedded in tissue freezing medium (Tissue-Tek) and 30 μm sections were cut. Sections were collected on glass slides and stored at −80°C.

For immunofluorescence experiments, we used an antigen retrieval kit from R&D Systems (catalog #CTS015). Sections were washed with TBS (3×/10 min) and placed in 1× retrieval buffer at 90°C for 10 min. Sections were then rinsed with TBS and incubated with 10% goat serum and 0.1% Tween 20 in TBS for 1 h at room temperature. Sections were then incubated with 2% goat serum and 0.1% Tween 20 in TBS containing rabbit anti-RCAN1 antibodies (1:1000; gift from Dr. Rejji Kuruvilla, Johns Hopkins University) or rabbit anti-CaN A-α antibodies 1:1000 (Millipore catalog #07-1492, RRID:AB_10563965) in combination with monoclonal mouse anti-pan-cadherin antibodies 1:200 (Abcam catalog #ab22744, RRID:AB_447300) overnight at 4°C. Sections were subsequently washed with TBS as described above and incubated with secondary antibodies (1:250, Alexa Fluor 488 goat anti-rabbit and Alexafluor 546 goat anti mouse; Invitrogen) for 1.5 h at room tem-

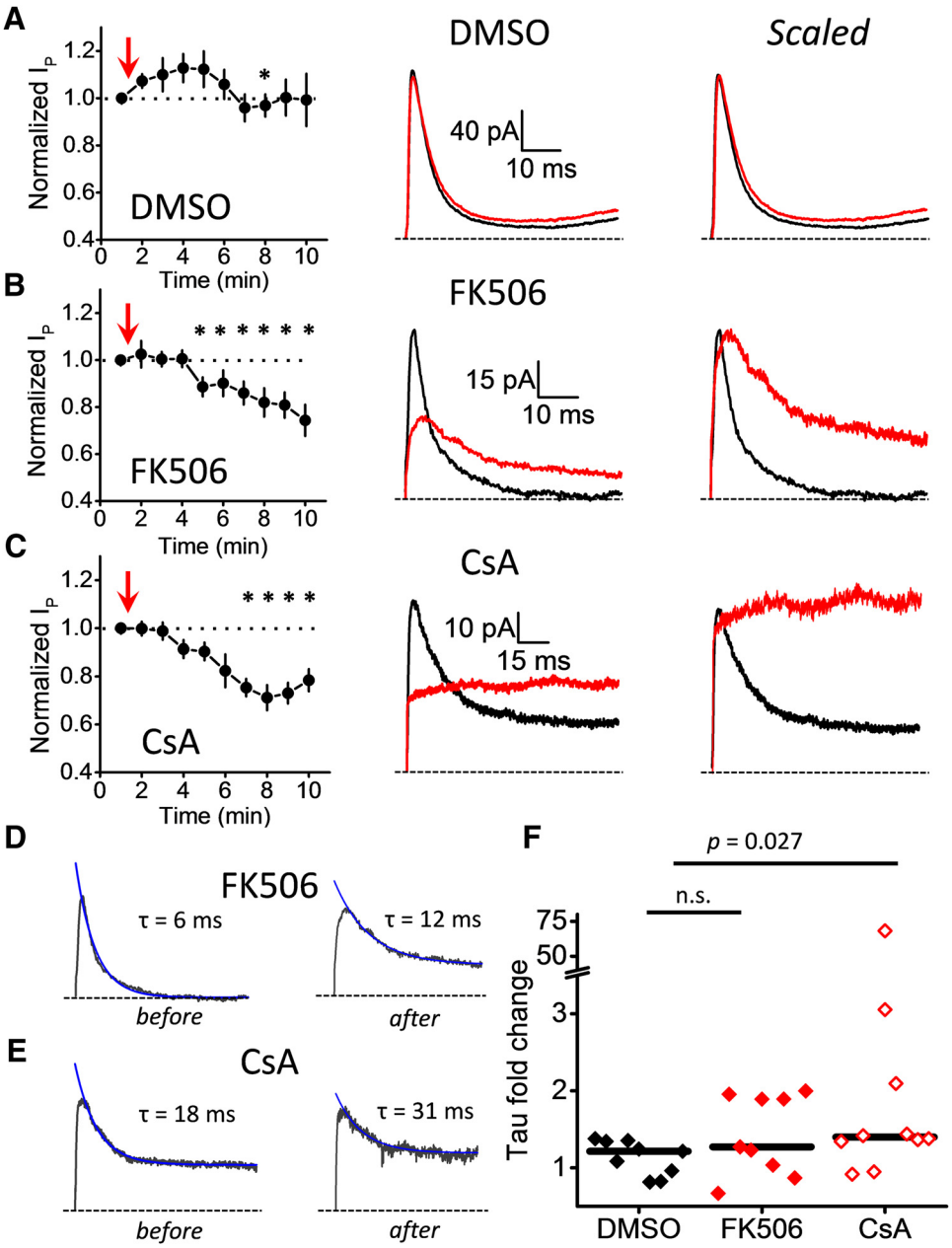

Figure 2. Attenuation of the Kv3.4 current and disruption of its inactivation profile upon inhibition of CaN in DRG neurons. ***A***, Time course of Kv3.4 peak current (I_P) at 1 min intervals after DMSO wash-in (left). From individual patches, the data point at 1 min is the average I_P from five sweeps before exposure to DMSO and subsequent data points are normalized snapshots of the I_P at the indicated times. The I_P is normalized to the average I_P from the first five sweeps before exposure to DMSO. The arrow represents the approximate time point of compound administration. The graph depicts the mean ± SEM from multiple patches ($n = 12$). Representative Kv3.4 current traces at baseline and after exposure to DMSO (center) are shown. Scaled currents are also shown (right). Patches were held at −100 mV before a step to −30 mV for 1 s followed by a test pulse to +80 mV for 500 ms before returning to −100 mV. The start-to-start interval was 12 s. ***B***, Same as ***A*** but with 1 μM FK506 ($n = 11$). ***C***, Same as ***A*** but with 10 μM CsA ($n = 11$). The Student's paired *t* test was used to evaluate statistically significant differences between the data at the 2 min time point and subsequent data points. *$p < 0.05$. ***D***, ***E***, Overlay of representative Kv3.4 currents and the corresponding best-fit exponential to the decay phase (blue line) before (left) and after (right) exposure to FK506 and CsA. ***F***, Dot plot comparing fold change in the inactivation time constant upon exposure to DMSO ($n = 14$), FK506 ($n = 10$; DF = 1; $\chi^2 = 1.03$), and CsA ($n = 11$; DF = 1; $\chi^2 = 4.86$). The horizontal black line represents the median value. The *p*-value is indicated in the graph (Kruskal–Wallis ANOVA).

perature before a final wash. Coverslips were added along with Prolong Gold Antifade Reagent with DAPI (Sigma-Aldrich). Confocal microscopy was performed at the Bioimaging Facility of the Sidney Kimmel Cancer Center (NIH Cancer Center Core Grant 5 P30 CA-56036). Images were then compiled and an individual blinded to the conditions quantified the mean fluorescence of individual cells from each section using ImageJ.

For quantification of differences in membrane staining, ImageJ was used to create fluorescence intensity plots by first tracing a straight line at a random angle through a 2D axis of each cell within a field of view by an individual blinded to the experimental conditions. The peak pan-cadherin mean fluorescence intensity (plasma membrane, two peaks) from a given *Z*-plane in each group was obtained and the mean fluorescence intensity of CaN was measured at the peaks. The CaN signal was then normalized to the peak pan-cadherin signal from that cell and the data were compared between groups (pan-cadherin signals did not differ between SCI and laminectomy groups). For quantification of cytoplasmic versus nuclear staining, borders were drawn around nuclei using the DAPI stain and around cells using the pan-cadherin stain. Mean fluorescence intensity was then gathered from either the nucleus or cytoplasm

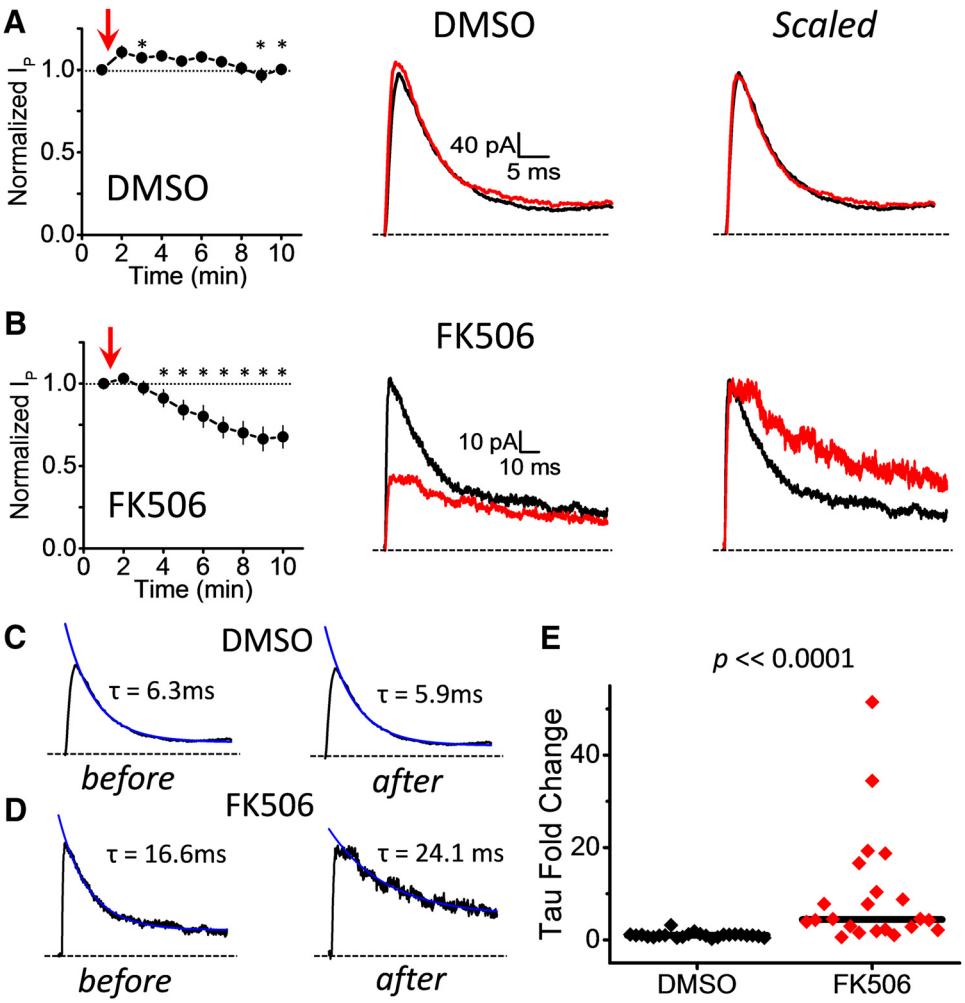

Figure 3. Attenuation of the Kv3.4 current and disruption of its inactivation profile upon inhibition of CaN in transfected CHO cells. ***A***, Time course of Kv3.4 peak current (I_P) at 1 min intervals after DMSO wash-in (left). The results were analyzed and plotted as described in the Figure 2 legend. The arrow represents the approximate time point of compound administration. The graph depicts the mean ± SEM from multiple patches ($n = 23$). Representative Kv3.4 current traces at baseline and after exposure to DMSO (center) are shown. Scaled currents are also shown (right). Patches were held at −80 mV before a 1 s test pulse to +50 mV followed by a return to −80 mV. The start-to-start interval was 12 s. ***B***, Same as ***A*** but with 10 μM FK506 ($n = 25$). Student's paired *t* test was used to evaluate statistically significant differences between the data at the 2 min time point and subsequent data points. *$p < 0.05$). ***C***, Overlay of representative Kv3.4 currents and the corresponding best-fit exponential to the decay phase (blue line) before (left) and after (right) exposure to DMSO. ***D***, Same as ***C*** but before and after exposure to FK506. ***E***, Dot plot comparing fold change in the inactivation time constant upon exposure to DMSO and FK506. The horizontal black line represents the median value. The *p*-value is indicated in the graph (Kruskal–Wallis ANOVA; $n = 24$ and 22, patches respectively; DF = 1; $\chi^2 = 24.70$).

and a ratio was calculated. Graphs and corresponding statistical analyses were produced in Origin Pro version 9.1 (OriginLab).

Before DRG transfections, both the expression of the RCAN1-Flag construct coupled with a testing of the anti-RCAN1 antibody were done in HEK293T cells. Cells were either mock transfected or transfected with the RCAN1-Flag construct. Individual coverslips from both groups were then stained with the rabbit anti-RCAN1 antibodies (1:1000, gift from Dr. Rejji Kuruvilla, Johns Hopkins University) and rabbit anti-Flag antibodies 1:1000 (Abcam catalog #ab1162, RRID:AB_298215), respectively. Only those cells transfected with the RCAN1-Flag construct and not mock transfected showed immunoreactivity to either the anti-Flag antibody or the anti-RCAN1 antibody.

Statistical analysis. Student's paired *t* test was used to evaluate paired datasets. The one-way ANOVA test was used to compare independent datasets if data passed tests for normality and equal variance (as determined by Levene's test). Otherwise, the Wilcoxon–Mann–Whitney or Kruskal–Wallis ANOVA tests were used. The Kolmogorov–Smirnov test was used to compare cumulative frequency histograms. Details of the statistical analysis are provided in the corresponding figure legends.

Results

CaN inhibitors broaden the AP waveform in putative nociceptors

Previously, we found that Kv3.4 siRNA prolongs the AP and decreases the maximum rate of repolarization in small-diameter DRG neurons (Ritter et al., 2012). To determine whether a similar relation exists after inhibition of CaN, we first examined the effects of two well established CaN inhibitors (FK506 and the auto-regulatory peptide inhibitor) on the AP of small-diameter DRG neurons (21.5 ± 0.4 μm, $n = 35$ somata; see Materials and Methods; Table 1). The vehicle (2% DMSO) did not affect AP amplitude, APD_{90}, or the maximal rates of depolarization and repolarization (Fig. 1*A–D*), but did have slight effects on the resting membrane potential, AP threshold, and afterhyperpolarization (Table 1). After a 5 min exposure to 10 μM FK506, the AP elicited by a 0.5 ms current injection pulse was significantly prolonged by 27% at APD_{90} in relation to paired controls recorded before application of the inhibitor (Fig. 1*G*, Table 1). Consistent

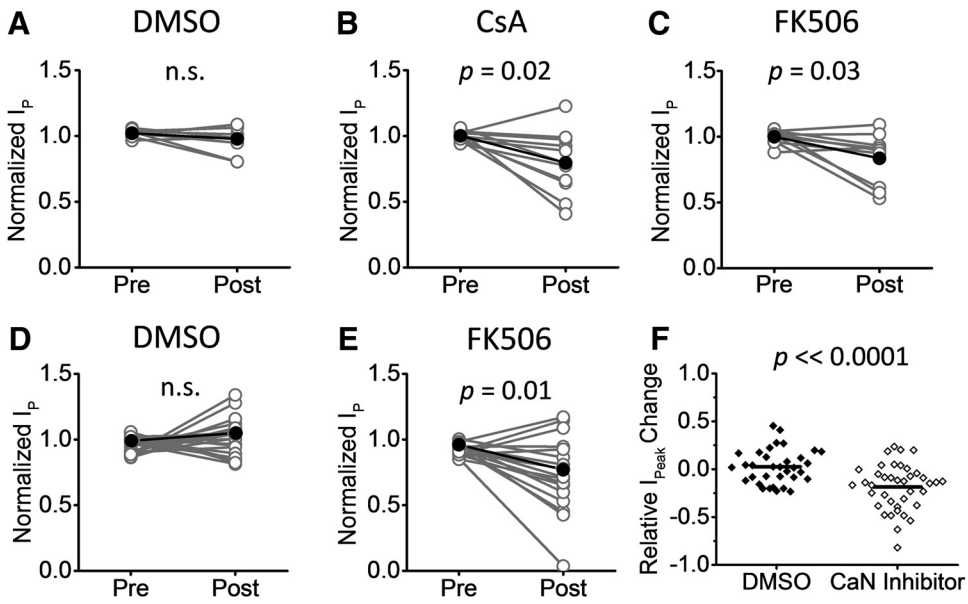

Figure 4. Attenuation of the total outward K^+ current upon inhibition of CaN in DRG neurons and CHO cells. ***A–C***, Paired scatter plot of the maximal peak outward K^+ currents recorded before and 10 min after applying DMSO, CsA, or FK506 to DRG neurons. Currents were evoked by a test pulse to +80 mV after a 20 s conditioning pulse to −140 mV. The normalized test pulse peak current is compared in the figure (paired Student's *t* test; $n = 10$; DF = 9; $t_{stat} = 0.80$, 11; DF = 10; $t_{stat} = 2.92$ and 9; DF = 8; $t_{stat} = 2.46$ patches, respectively). ***D***, ***E***, Paired scatter plot of the maximal peak outward K^+ currents recorded before and 10 min after washing DMSO or FK506 onto CHO cells expressing Kv3.4. Currents were evoked by a test pulse to +70 mV after a 20 s conditioning pulse to −140 mV. The normalized test pulse peak current is compared in the figure (paired Student's *t* test; $n = 18$; DF = 17; $t_{stat} = 2.92$ and 23; DF = 22; $t_{stat} = 1.53$ patches, respectively). ***F***, Combined data of the peak current change in ***A–E*** to compare the effects of CaN inhibitors and DMSO globally. The *p*-value is indicated in the graph (one-way ANOVA; $n = 42$ and 29, respectively; DF = 1; F = 18.01).

with the broadening, the maximum rate of AP repolarization decreased to 77% of control (Fig. 1*H*, Table 1). In addition, the AP amplitude and maximum rate of AP depolarization were modestly reduced upon exposure to FK506 (Table 1). FK506 inhibits CaN indirectly through its binding to FKBP12 and might have off-target effects (Richter et al., 1995; Ahn et al., 2007; Sachewsky et al., 2014). To verify that the effects of FK506 on the AP waveform resulted from inhibition of CaN, we also examined the effects of the CaN auto-regulatory peptide, which inhibits the phosphatase directly (Hashimoto et al., 1990). This peptide, however, does not cross the cell membrane. Therefore, peptide freshly dissolved in the intracellular solution at a final concentration of 50 μM was included in the patch pipette and delivered into the neuron upon establishing the whole-cell configuration. The first AP was then recorded 10 min later ("control") and subsequent recordings were taken at intervals of 5 min (at least two more AP recordings after the initial 10 min control). The effects of the CaN auto-regulatory peptide on the AP waveform were qualitatively similar to those of FK506 (Fig. 1*I–L*, Table 1). It also significantly prolonged the AP (41% longer at APD_{90}) and slowed the maximum rates of depolarization and repolarization (80% and 71% of control, respectively). In addition, it had a modest depolarizing effect on the afterhyperpolarization ($\Delta V = +4.8$ mV). Both FK506 and the auto-regulatory peptide inhibitor had no effect on the resting membrane potential, input resistance, or AP threshold (Table 1). Overall, these results demonstrate that CaN inhibition modulates the AP waveform by consistently slowing the maximum rates of depolarization and repolarization, which broadens the AP. Focusing on the Kv3.4 channel as a major regulator of AP repolarization in small-diameter DRG neurons (Ritter et al., 2012), we investigated the effects of CaN inhibition on the Kv3.4 current.

CaN inhibition attenuates the Kv3.4 current and slows its fast inactivation profile

To determine whether attenuation of the Kv3.4 current contributes to the modulation of the AP by CaN inhibition, we examined cell-attached patches from acutely dissociated small-diameter DRG neurons as described previously (see Materials and Methods). Under these conditions, we have previously observed robust macroscopic Kv3.4 currents exhibiting fast inactivation (Ritter et al., 2012). At intervals of 12 s (start to start), we evoked the current by a step depolarization to +80 mV after a 1 s conditioning pulse to −30 mV to inactivate low voltage-activating A-type K^+ currents (Fig. 2). The vehicle (2% DMSO) only induced a slight early upregulation, but the current returned to pretreatment levels at later time points (Fig. 2*A*). In contrast, upon exposing the neurons to 1 μM FK506 or 10 μM CsA, the peak current underwent significant time-dependent attenuation after a delay of ~5 min (Fig. 2*B*,*C*). Furthermore, this attenuation was accompanied by a significant slowing of fast inactivation of the Kv3.4 current (Fig. 2*D–F*). Accordingly, the time constant of current decay changed more in the CaN-inhibitor-treated groups than in the DMSO groups; however, statistical significance was only found when comparing DMSO and CsA. The median baseline inactivation time constant was 14.29 ms and ranged between 6.09 and 110.36 ms. The median fold change and range were as follows: DMSO, 1.2 (0.81, 1.38); CsA, 1.4 (0.92, 68.2); and FK506, 1.2 (0.67, 2). Observing qualitatively similar effects of FK506 and CsA on the Kv3.4 current strongly supports the role of CaN because these inhibitors have distinct mechanisms of action (Liu et al., 1991). These results demonstrate that maintenance of the Kv3.4 current and its fast inactivating profile in putative nociceptors depend on CaN activity. In addition, we found that 10 μM FK506 has very similar effects on the current

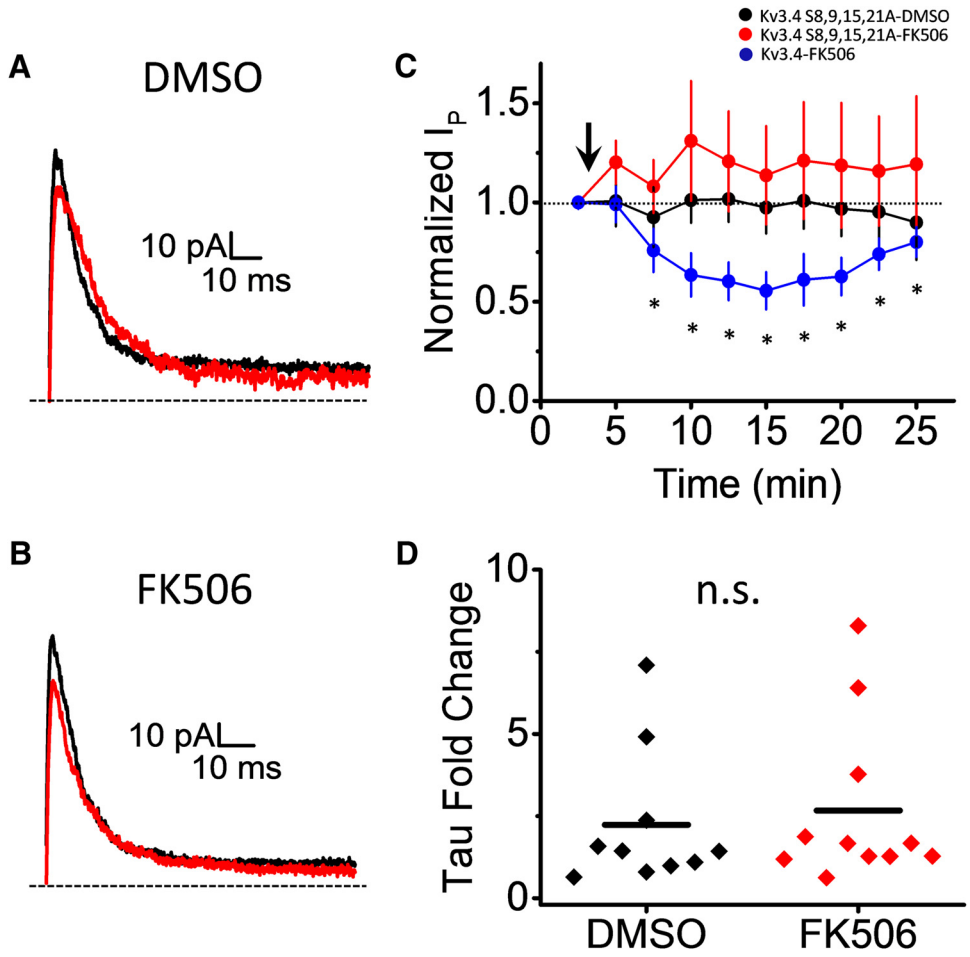

Figure 5. Mutation of N-terminal serines 8, 9, 15, and 21 to alanines eliminates CaN inhibitor-induced modulation of the Kv3.4 current. ***A***, Representative current trace of Kv3.4 N-terminal alanine mutant at baseline and after exposure to DMSO. Patches were held at −80 mV before a 1 s test pulse to +50 mV followed by return to −80 mV. To account for the slower recovery from inactivation of the alanine mutant, the start-to-start time was 30 s. ***B***, Same as ***A*** but with exposure to 10 μM FK506. ***C***, Time course of Kv3.4-alanine mutant peak current (I_P) at ~2.5 min intervals after DMSO wash-in (black) and FK506 wash-in (red). The wild-type Kv3.4 was also tested (blue). The arrow represents the approximate time point of compound administration. Data were analyzed as described in Fig. 2 legend. *$p < 0.05$ (Student's paired t test; $n = 11$, 15 and 6, respectively). ***D***, Dot plot comparing fold change in the inactivation time constant of the alanine mutant upon exposure to DMSO and FK506. The horizontal black line represents the mean value (one-way ANOVA; $n = 10$ and 11, respectively; DF = 1; $F = 0.18$).

induced by recombinant Kv3.4 channels heterologously expressed in CHO cells, whereas the vehicle had little to no effect on the peak current or the time constant of inactivation (Fig. 3). The median fold change and range were as follows: DMSO 0.99 (0.21, 3.18) and FK506, 4.41 (0.58, 51.49).

As mentioned previously, the test pulse that evokes the Kv3.4 currents is delivered from a conditioning pulse to −30 mV. Therefore, it was important to verify that the total outward K^+ current was reduced due to the attenuation of Kv3.4. The I_{max}, at a hyperpolarized conditioning voltage that is expected to recruit all available Kv3.4 channels (i.e., −140 mV), was not affected by the vehicle, but was significantly reduced in the presence of FK506 or CsA in DRG neurons (~80% of control; Fig. 4*A–C*). We confirmed this result with the recombinant Kv3.4 heterologously expressed in CHO cells (Fig. 4*D*,*E*).

Phosphorylation sites within the Kv3.4 NTID are responsible for Kv3.4 dysfunction induced by CaN inhibition

PKC-dependent phosphorylation at four sites (S8, S9, S15, and S21) within the Kv3.4 NTID, and the resulting conformational change, disrupt fast N-type inactivation of the Kv3.4 channel (Covarrubias et al., 1994; Beck et al., 1998; Antz et al., 1999). We investigated whether phosphorylation of these sites might also underlie Kv3.4 current attenuation in response to CaN inhibition. Phosphorylation and desphosphorylation of the NTID might occur under basal conditions. The balance between the basal activities of PKC and CaN would then determine the phosphorylation state of the NTID. Therefore, dephosphorylation of these sites by CaN would be necessary, not only to preserve the fast inactivating profile of the Kv3.4 current, but also to maintain a robust Kv3.4 current in DRG neurons. To investigate a novel role of the aforementioned phosphorylation sites, we tested the effect of CaN inhibition by FK506 on the current generated by the Kv3.4 channel with all four N-terminal serines mutated to alanine (Fig. 5). We expressed both wild-type and mutant Kv3.4 channels in CHO cells and tested the effects of FK506 under identical conditions. The Kv3.4 wild-type current exhibited attenuation and disrupted inactivation upon CaN inhibition, as described previously (Figs. 2, 3). In contrast, the peak current generated by the mutant Kv3.4 channel underwent little to no change upon exposure to FK506 or vehicle alone (Fig. 5*A–C*). The vehicle and FK506 results were indistinguishable. There was no significant change between the alanine mutant groups when using paired data within one group (i.e., alanine mutant patches exposed to FK506 over time) or when comparing datasets at dis-

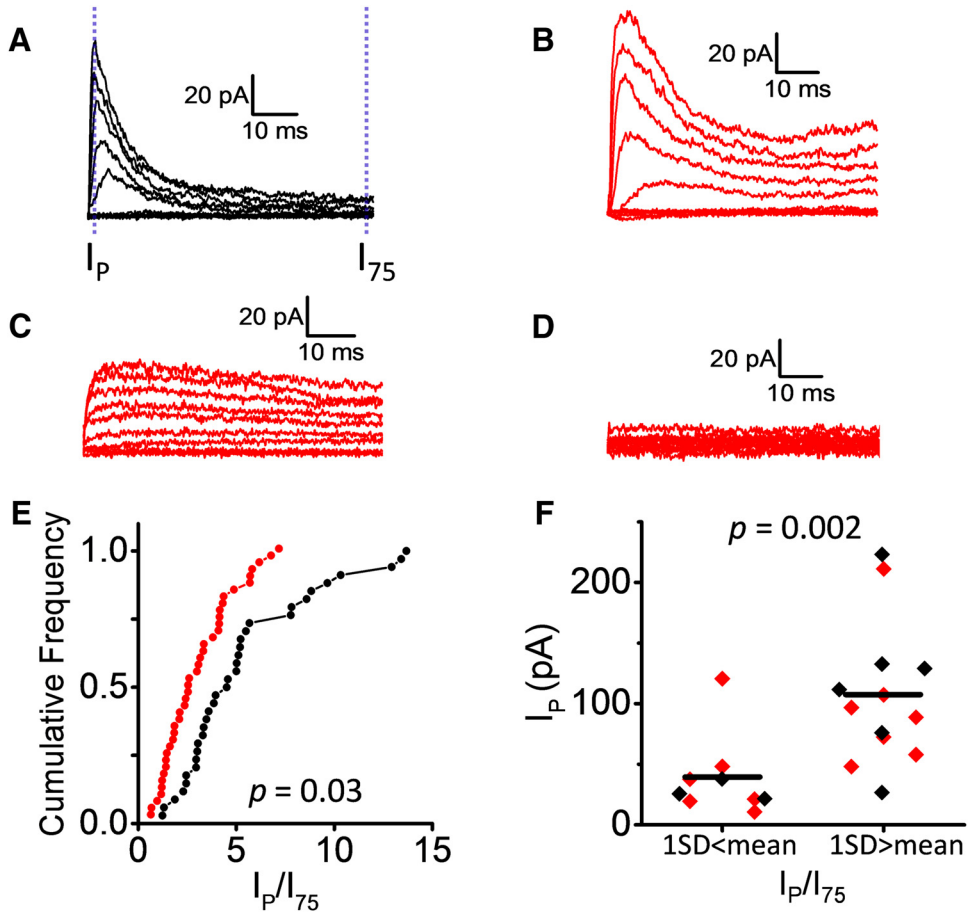

Figure 6. Kv3.4 current in small-diameter DRG neurons exhibits attenuation and disrupted inactivation after SCI. ***A–D***, Representative families of cell-attached high-voltage-activating outward K^+ currents from laminectomy (black) and SCI neurons (red) 2 weeks after surgery. Currents were evoked by step depolarizations starting at −80 mV and ending at +100 mV at 20 mV intervals. From a holding potential of −100 mV, all test pulses were preceded by conditioning pulse to −30 mV to inactivate low-voltage-activating K^+ currents. The protocol's start to start was 12 s. ***E***, Cumulative frequency histograms comparing the I_p/I_{75} ratio from the laminectomy and SCI groups (n = 34 and 40 patches, respectively). As shown in ***A***, this ratio measures the degree of inactivation by comparing the peak current (I_p) with the current at 75 ms after the onset of the step depolarization (dashed line markings). At 75 ms, macroscopic Kv3.4 inactivation is typically maximal under basal naive conditions (Ritter et al., 2012). The Kolmogorov–Smirnov test was used to evaluate the difference between the cumulative frequency histograms (p-value is indicated in the graph). ***F***, Comparison of the peak outward currents one SD away from the mean from combined laminectomy (black) and SCI (red) groups (n = 22: 13 inactivating currents and 9 noninactivating currents; DF = 1; $\chi^2 = 9.23$). If the $I_p/I_{75} \geq 1$ SD > the mean, then inactivation is profound. In contrast, if the $I_p/I_{75} \geq 1$ SD < the mean, then inactivation is profoundly disrupted. The horizontal black lines represent the medians of each group. The p-values are indicated in the graphs (Kruskal–Wallis ANOVA).

tinct time points between the groups (i.e., DMSO vs FK506 exposed patches at a given time point). Furthermore, the changes in macroscopic inactivation of the mutant Kv3.4 current induced by exposure to either vehicle or FK506 were also generally small or negligible (Fig. 5*D*). In a few instances, upon exposure to either vehicle or FK506, spontaneous disruption of inactivation could have resulted from previously described cysteine oxidation in the absence of NTID phosphorylation sites (Fig. 5*D*) (Ruppersberg et al., 1991; Duprat et al., 1995). These results demonstrate that Kv3.4 NTID phosphorylation sites play a novel role in maintaining a robust basal level of the Kv3.4 current in a manner that depends on CaN activity.

SCI induces Kv3.4 dysfunction that mirrors the effects of CaN inhibition

To assess the role of CaN inhibition on the SCI-induced dysregulation of the DRG Kv3.4 current, we first examined the properties of the Kv3.4 current in cell-attached patches from small-diameter DRG neurons after either a laminectomy (sham surgery control) or a unilateral cervical contusion that results in persistent neuropathic pain-related behaviors (Materials and Methods; Fig. 6). As reported previously, we found that the Kv3.4 current undergoes modulation of fast inactivation under SCI conditions (Ritter et al., 2015a). Whereas the neurons from the laminectomy group mainly express robust fast inactivating outward currents, those from the SCI group displayed highly variable outward currents with more diverse phenotypes: fast inactivating, slow inactivating, and noninactivating (Fig. 6*A–C*). Patches with negligible outward currents were also observed in this group (Fig. 6*D*). To assess quantitatively the degree of inactivation of the currents, we measured the ratio of the peak outward current to the magnitude of the current at 75 ms, the time at which most of the fast inactivating Kv3.4 current under basal conditions would be inactivated (I_P/I_{75}; Fig. 6*A*). Demonstrating that modulated Kv3.4 currents in the SCI group have disrupted fast inactivation, we found that the I_P/I_{75} was significantly reduced compared with the ratio from currents in the laminectomy group (Fig. 6*E*). Then, to determine whether the slowest inactivating currents were associated with small peak currents, we compared currents with I_P/I_{75} at least 1 SD greater than the mean (currents dominated by fast inactivation) to those with I_P/I_{75} at least 1 SD smaller than the mean (currents dominated

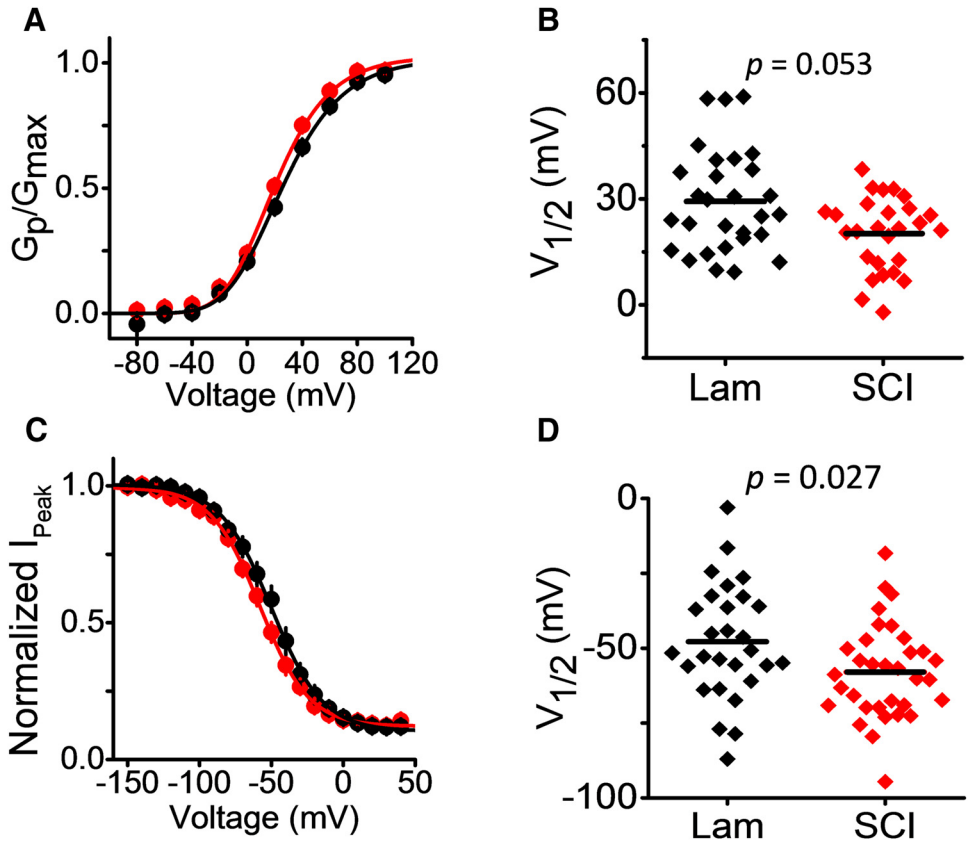

Figure 7. SCI induces minimal changes on Kv3.4 biophysical properties. ***A***, Normalized G_p–V relation from laminectomy (black) and SCI (red) 2 weeks after surgery. Pulse protocol is as described in Figure 5 legend ($n = 29$ and 27 cells for laminectomy and SCI groups, respectively). Solid lines are best-fit fourth-order Boltzmann functions (Materials and Methods). ***B***, Scatter plot of $V_{1/2}$ values extracted from individual G_p–V relations 2 weeks after laminectomy and SCI. Horizontal bars indicate means. (one-way ANOVA; DF = 1; $F = 3.89$) ($V_{1/2}$ mean ± SEM; laminectomy = +27.45 ± 2.67; SCI = +20.25 ± 2.49). ***C***, Steady-state inactivation curves 2 weeks after laminectomy (black) and SCI (red) ($n = 28$ and 33, respectively). The solid lines are best-fit Boltzmann functions. Currents were evoked by a test pulse to +80 mV after 20 s conditioning pulses starting at −150 mV and ending at +50 mV. The interval between conditioning pulses was 10 mV and the patch was held at −100 mV for 20 s before delivering the next conditioning pulse (to ensure recovery from inactivation). ***D***, Scatter plot of $V_{1/2}$ values derived from individual steady-state inactivation curves 2 weeks after laminectomy and SCI. Horizontal bars indicate mean values. The *p*-values are indicated in the graphs (one-way ANOVA; DF = 1; $F = 5.12$) ($V_{1/2}$ mean ± SEM; laminectomy = −47.59 ± 3.66; SCI = −60.0 ± 2.89).

by slow inactivation). These results show that currents with profound inactivation show significantly larger peaks compared with those with little or no inactivation regardless of the group from which they were measured (SCI vs laminectomy) (Fig. 6*F*). Consistent with the effects induced by CaN inhibition (Fig. 2–4), we found that, whereas smaller peak currents with disrupted inactivation are mostly from the SCI group (6/9 patches; Fig. 6*F*), only ~50% of patches from the SCI group are in the category of larger currents displaying profound inactivation (7/13 patches; Fig. 6*F*). These results demonstrate that SCI and CaN inhibition induce similar effects on the Kv3.4 current in DRG neurons by attenuating the peak current and disrupting macroscopic inactivation.

We also observed that, whereas the Kv3.4 peak conductance–voltage curve ($G_{peak} - V$ curve) was not affected by SCI ($V_{1/2}$; laminectomy = +27.45 ± 2.67; SCI = +20.25 ± 2.49; $p = 0.053$), the steady-state inactivation curve was slightly leftward shifted in the SCI group ($V_{1/2}$; laminectomy = −47.59 ± 3.66; SCI= −60.0 ± 2.89; $p = 0.027$) relative to those in the laminectomy group (Fig. 7*A–D*). The leftward-shifted steady-state inactivation curve could decrease the available Kv3.4 current at steady state in the relevant membrane potential range (−70 to −40 mV) and therefore contribute to Kv3.4 current attenuation.

SCI induces upregulation of the RCAN1 in DRG neurons

Because CaN inhibition modulates the Kv3.4 current of DRG neurons in two major ways that mirror SCI-induced dysregulation of this current (smaller peak and reduced inactivation), we hypothesized that SCI might inhibit CaN activity in the DRG. Therefore, we investigated whether CaN expression had been affected by SCI. Immunofluorescence staining of the catalytic subunit, CaN Aα, demonstrated localization at the plasma membrane, diffuse cytoplasmic staining, and punctate nuclear staining (Fig. 8*A*). Although the overall DRG immunofluorescence intensity per cell was 21% greater in the SCI group (laminectomy median and range (arbitrary units) = 338 (84, 700); SCI median and range (arbitrary units) = 428 (42, 853), $p = 5.6 \times 10^{-13}$), we observed no significant difference in plasma membrane expression, the nuclear to cytoplasmic ratio, or the number of nuclear puncta per cell per section (Fig. 8*B–E*). Therefore, SCI does not induce CaN Aα downregulation or redistribution in DRG neurons. Based on the results above, we reasoned that, rather than changing CaN protein expression or localization, SCI may induce upregulation of endogenous modulators of CaN activity. Specifically, upregulation of RCAN1 in the DRG could inhibit CaN after SCI. RCAN1 is abundantly expressed in the nervous system and is upregulated in many neurological disorders, including

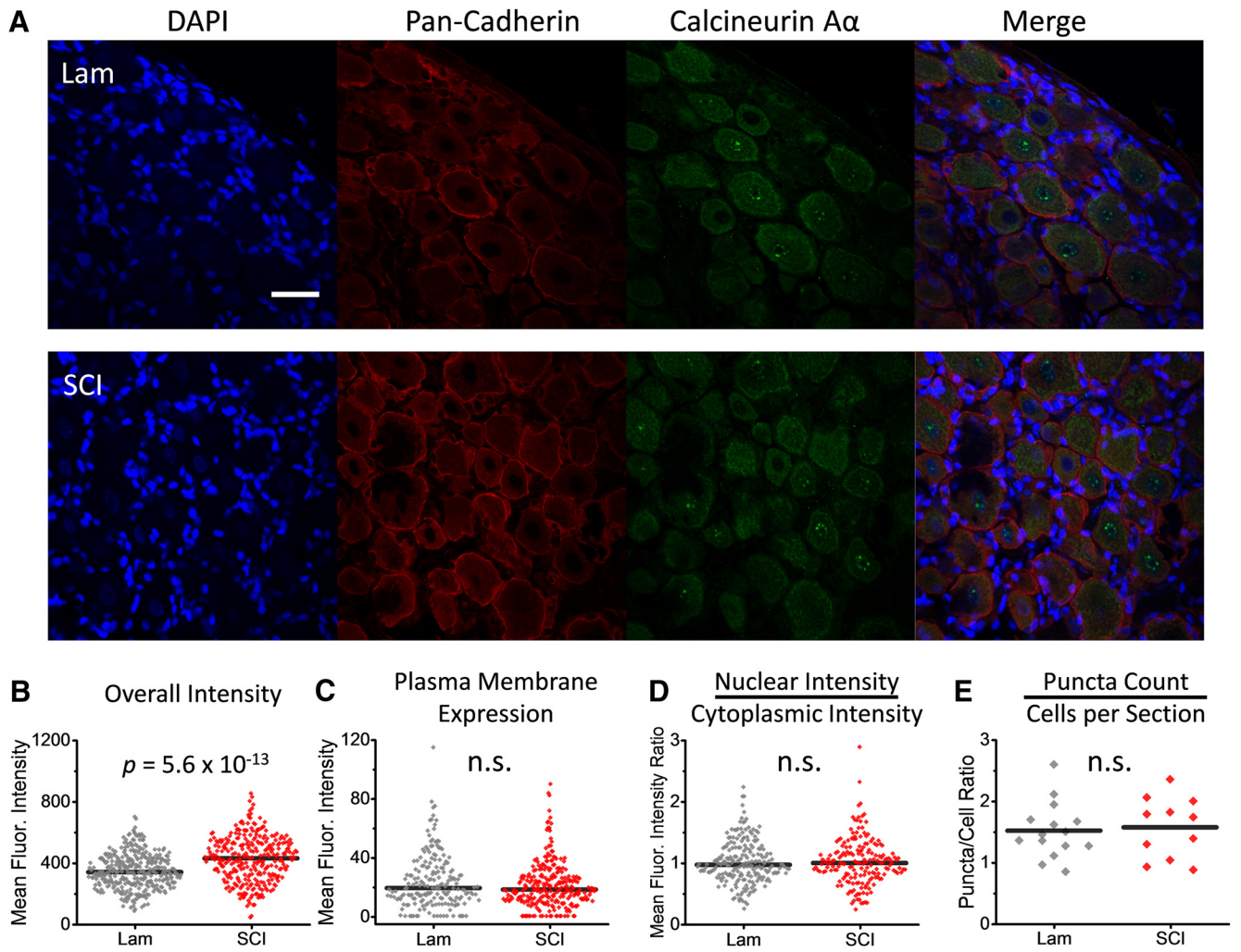

Figure 8. SCI has little to no effect on CaN Aα expression and localization in the DRG. ***A***, Immunostaining of CaN Aα (green) counterstained with DAPI (blue), and pan-cadherin (red) in DRGs from rats that received either SCI or laminectomy. Scale bar represents 60 μm. ***B***, Dot plot comparing average CaN staining intensity from individual DRG neurons in the SCI and laminectomy groups (n = 309 and 354 cells, respectively; DF = 1; $\chi^2 = 52$). ***C***, Dot plot comparing mean CaN staining intensity at neuronal plasma membranes as measured by pan-cadherin colocalization in the SCI and laminectomy groups (n = 278 and 192 cells, respectively; DF = 1; $\chi^2 = 1.15$). ***D***, Dot plot comparing the ratio of nuclear versus cytoplasmic average fluorescence intensity of CaN as determined by colocalization with DAPI (nuclear) and cytoplasm from SCI and laminectomy groups (n = 214 and 184 cells, respectively; DF = 1; F = 0.04). The average fluorescence intensity of the cytoplasmic CaN includes the area of the cell enclosed by the pan-cadherin signal (plasma membrane) but excluding the nucleus (DAPI stain). The nuclear CaN expression was defined as the CaN signal that overlapped with the DAPI signal. ***E***, Dot plot comparing the ratio of the number of puncta from a given tissue section to the number of cells within that section from SCI and laminectomy (n = 11 and 15 sections, respectively; DF = 1; F = 0.08). Significant p-values are indicated in the graphs [Kruskal–Wallis ANOVA; n = 2 rats (11 sections) and 3 rats (15 sections) in the SCI and laminectomy groups for all experiments stated above, respectively].

Alzheimer's disease, stroke, and Down syndrome (Cho et al., 2008; Patel et al., 2015; Kipanyula et al., 2016; Lee et al., 2016). After SCI, RCAN1 is also upregulated in the rat spinal cord (Wang et al., 2016). To test the role of RCAN1 in the SCI-induced dysregulated Kv3.4 function in the DRG, we first investigated the effect of unilateral cervical SCI on RCAN1 expression at the mRNA and protein levels in DRG sections ipsilateral to the injury using FISH and RCAN1 immunostaining, respectively (for antibody validation, see Materials and Methods). Whereas DRG satellite cells displayed negligible RCAN1 mRNA expression, we observed distinct mRNA puncta in the somata of individual DRG neurons throughout the tissue (Fig. 9). Two weeks after surgery, we found significantly increased RCAN1 mRNA levels in DRG neurons (56% increase; $p = 0.008$) from rats in the SCI group compared with the laminectomy control group (Fig. 9*A*,*C*). Furthermore, we found a corresponding increase in RCAN1 immunoreactivity (27% increase; $p = 3.9 \times 10^{-15}$) in individual DRG neurons from the SCI group (Fig. 9*B*,*D*). These results demonstrate that SCI-induced RCAN1 upregulation could be responsible for Kv3.4 dysfunction through inhibition of CaN.

RCAN1 overexpression in DRG neurons attenuates the Kv3.4 current, disrupts Kv3.4 inactivation, and alters AP trajectory

To determine whether RCAN1 could be responsible for the SCI-induced attenuation of the Kv3.4 current in DRG neurons, we overexpressed a RCAN1-Flag construct in these neurons (for construct validation, see Materials and Methods). Once immunostaining confirmed the expression of RCAN1-Flag (Fig. 10*A*), we investigated Kv3.4 currents of DRG neurons transfected with EGFP alone or cotransfected with RCAN1-Flag and EGFP (Fig. 10*B*,*C*, respectively). Cumulative frequency histograms show that, compared with mock-transfected neurons (EGFP alone), RCAN1-Flag-expressing neurons displayed an excess of smaller Kv3.4 currents (Fig. 10*E*). In addition, the degree of inactivation (I_P/I_{75}) was also reduced significantly (Fig. 10*D*). These observa-

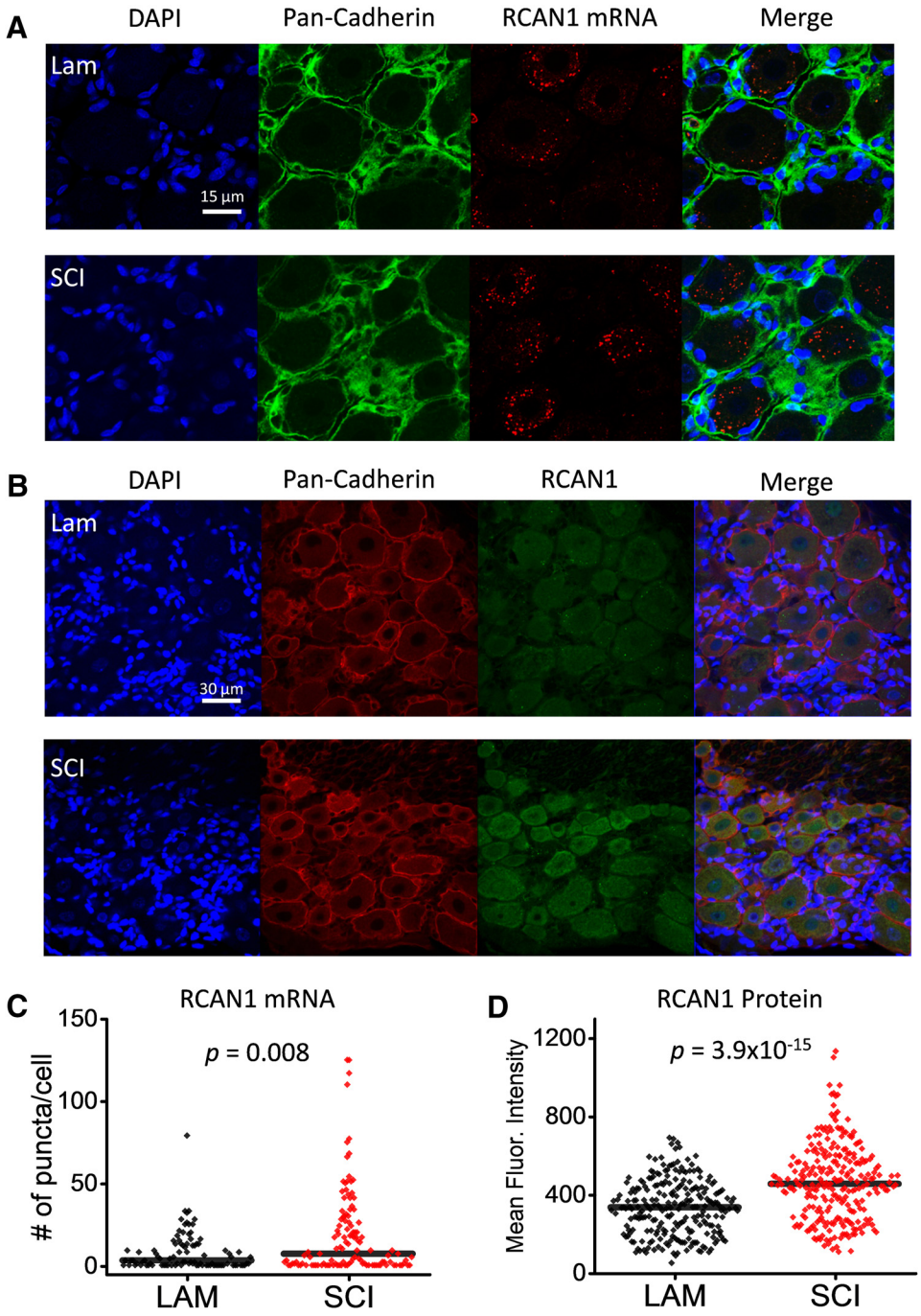

Figure 9. SCI induces upregulation of RCAN1 at the mRNA and protein levels in DRG neurons. ***A***, FISH analysis of RCAN1 mRNA expression (red) in DRGs from rats that received either SCI or laminectomy. DRG sections were counterstained with DAPI (blue) and pan-cadherin (green). ***B***, Immunostaining of RCAN1 protein (green) counterstained with DAPI (blue) and pan-cadherin (red) in DRGs from rats that received either SCI or laminectomy. ***C***, Quantification of RCAN1 mRNA puncta in DRG neurons from rats that received laminectomy or SCI ($n = 95$ and 121 neurons, respectively; DF = 1; $\chi^2 = 7.0$). ***D***, Quantification of RCAN1 immunofluorescence in DRG neurons from rats that received laminectomy or SCI ($n = 264$ and 260 neurons, respectively; DF = 1; $\chi^2 = 61.73$). The *p*-values are indicated in the graphs (Kruskal–Wallis ANOVA; $n = 3$ and 3 SCI and laminectomy rats, respectively).

tions recapitulate the effects of CaN inhibitors (FK506 and CsA) and SCI on the Kv3.4 current (Figs. 2, 3). Therefore, there is a plausible link among SCI-induced RCAN1 upregulation, CaN inhibition, and Kv3.4 attenuation accompanied by disrupted fast inactivation.

We then investigated whether the extent of Kv3.4 current attenuation induced by RCAN1 overexpression is sufficient to recapitulate the effects of CaN inhibitors on the trajectory of the AP in DRG neurons (Fig. 1). We found that the APD_{90} [median and ranges: EGFP, 0.93 ms (0.35, 1.45); EGFP + RCAN1-Flag, 0.97 ms (0.61, 1.08); $n = 11$ and 14 respectively; Kruskal–Wallis ANOVA; $p = 0.38$] and the maximum rate of repolarization of the APs (median and ranges: EGFP 34.01 (17.44, 118.58); EGFP + RCAN1-Flag, 32.69 (25.29, 58.42); $n = 11$ and 14, respectively; Kruskal–Wallis ANOVA; $p = 0.44$) under control and RCAN1 overexpression conditions were indistinguishable. Therefore, the extent to which acute RCAN1 overexpression in DRG neurons attenuates the Kv3.4 current is insufficient to change

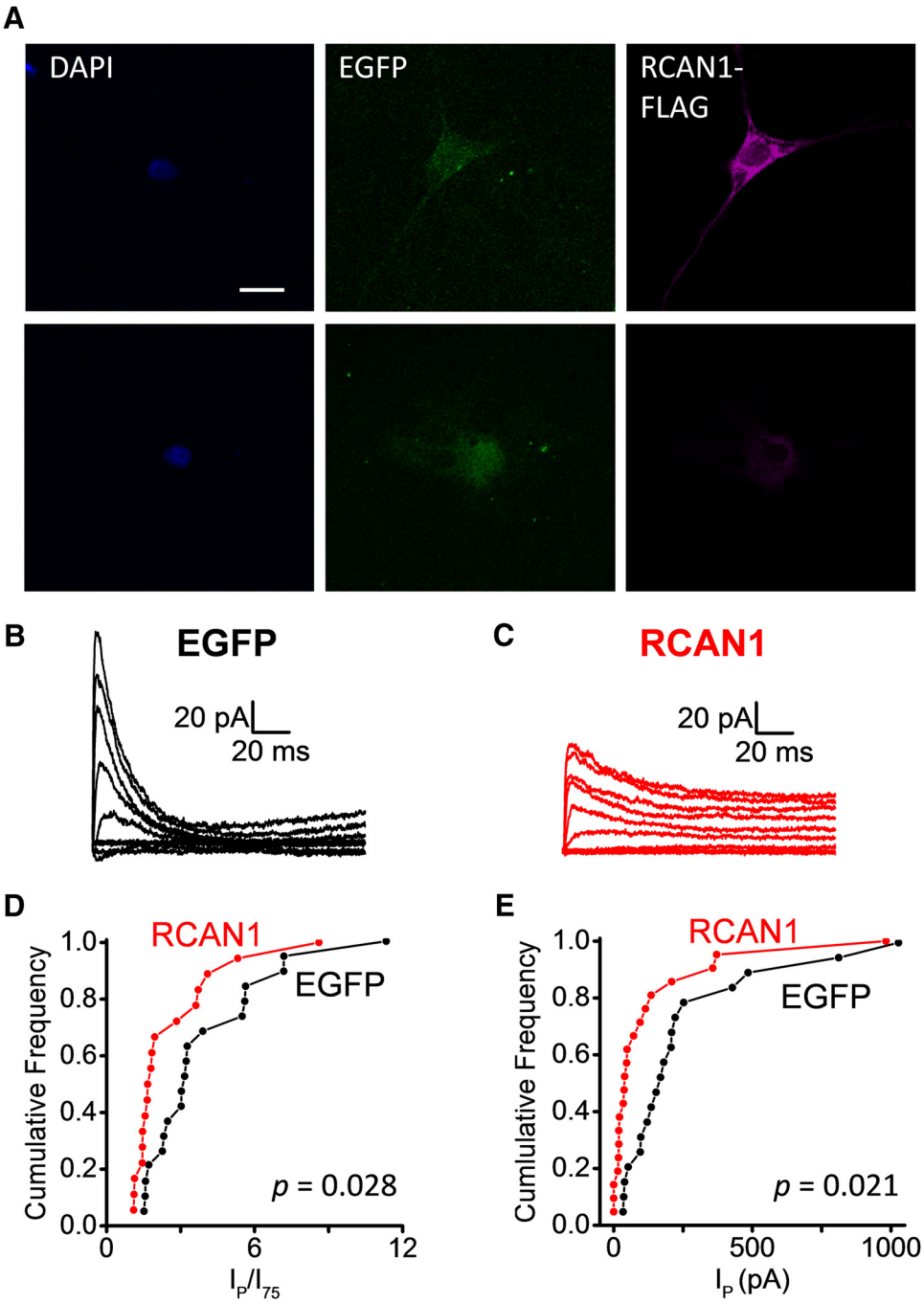

Figure 10. RCAN1 overexpression in DRG neurons attenuates Kv3.4 peak currents and inactivation. ***A***, Anti-Flag immunostaining (magenta) of a DRG neuron transfected with EGFP (bottom right) and a DRG neuron transfected with the fusion construct RCAN1-Flag + EGFP (top right). Scale bar, 20 μm. EGFP fluorescence (green) and DAPI counterstaining (blue) are also shown (center and left, respectively). ***B***, ***C***, Families of currents evoked as described in Figure 5 legend. ***D***, ***E***, Cumulative frequency histograms of the I_P/I_{75} and I_P from either EGFP (black) or EGFP + RCAN1-Flag (red) transfected neurons. The *p*-values are indicated in the graphs (Kolmogorov–Smirnoff test; $n = 19$ and 18 patches, respectively).

repolarization of the AP. However, the coefficients of variation of the APD_{90} (EGFP = 0.41; RCAN1-Flag = 0.20) and the maximum rate of repolarization (EGFP = 0.65; RCAN1-Flag = 0.27) are decreased upon RCAN1-Flag expression, suggesting a reduced ability to regulate the AP.

In the light of this result, we resorted to rat embryonic DRG neurons in culture to optimize the overexpression of RCAN1 and the effects on the Kv3.4 current. Compared with those from adults, embryonic DRG neurons allow improved transfection efficiency and survival after nucleofection. Within ~16 h after nucleofection, we detected a 1.87-fold increase in RCAN1-Flag expression (Fig. 11*A*). These neurons also expressed a robust high-voltage-activating A-type current with biophysical properties similar to those of DRG neurons from pups and adults (Fig. 11*B*). Moreover, as shown previously for DRG neurons from pups, Kv3.4 siRNAs nearly abolished the embryonic Kv3.4 current (Ritter et al., 2012). However, compared with the results from adult DRG neurons, RCAN1 overexpression in embryonic DRG neurons had a greater effect on the Kv3.4 current (Fig. 11*B*,*C*). Cumulative frequency histograms revealed that, compared with mock-transfected neurons (EGFP alone), RCAN1-Flag expressing neurons displayed a significant excess of smaller

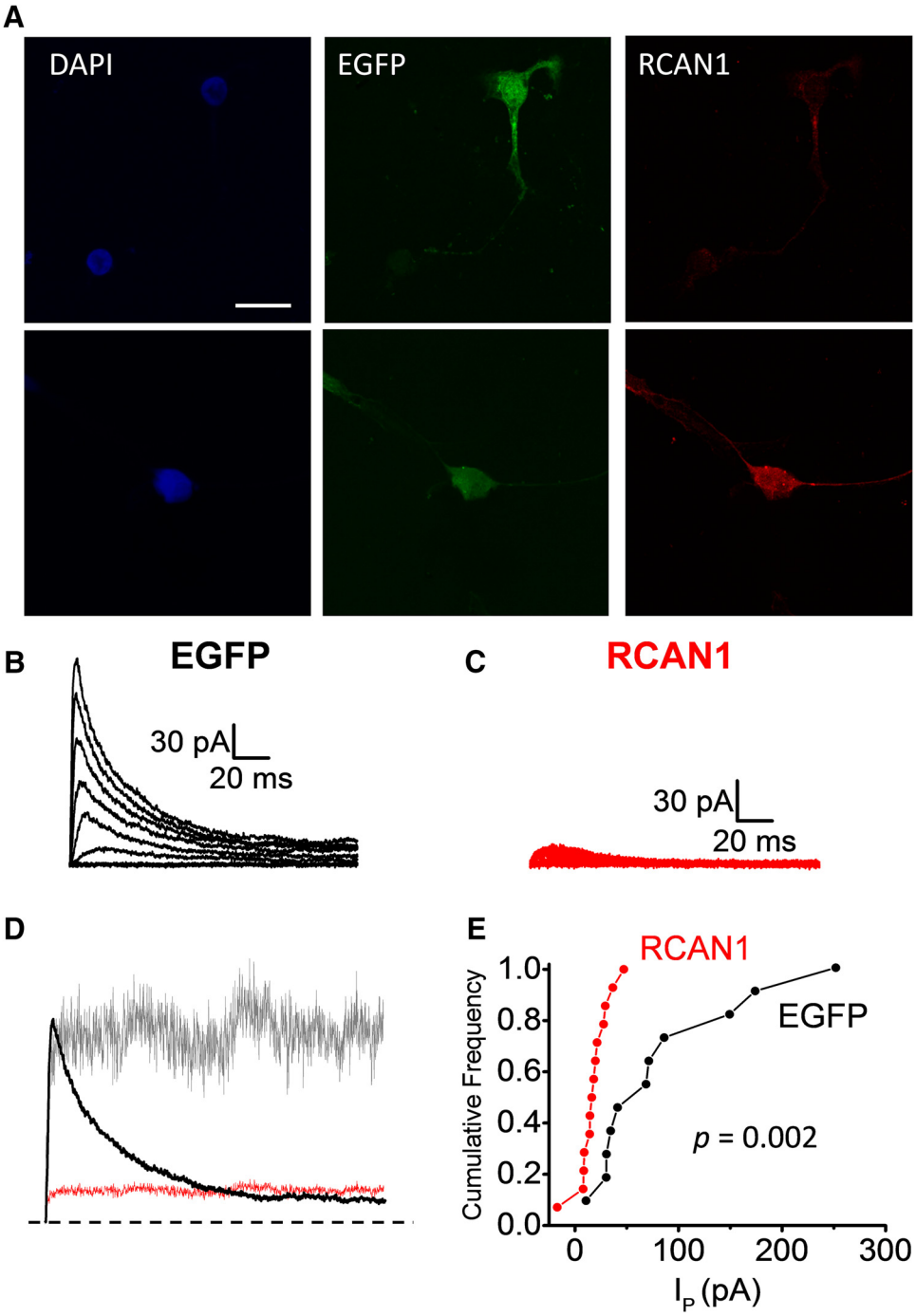

Figure 11. RCAN1 overexpression in embryonic DRG neurons nearly eliminates Kv3.4 currents and disrupts inactivation. ***A***, Anti-RCAN1 immunostaining (red) of a DRG neuron transfected with control plasmid + EGFP (top, right) and a DRG neuron transfected with the fusion construct RCAN1-Flag + EGFP (bottom, right). EGFP fluorescence (green) and DAPI counterstaining (blue) are also shown (center and left, respectively). Scale bar, 30 μm. ***B***, ***C***, Families of currents evoked as described in Figure 5 legend. ***D***, EGFP and RCAN1 currents (black and red respectively) and the scaled RCAN1 current (grey). ***E***, Cumulative frequency histograms of I_p from either control plasmid + EGFP (black) or RCAN1-Flag + EGFP (red) transfected neurons. The *p*-value is indicated in the graph (Kolmogorov–Smirnoff test; $n = 11$ and 14 patches, respectively).

Kv3.4 currents (Fig. 11*E*). Although these currents were too small to derive inactivation time constants reliably, there were instances of small currents displaying severely disrupted inactivation (Fig. 11*D*). We then compared the APs from mock-transfected neurons against those from RCAN1-Flag-transfected neurons (Fig. 12). As found with CaN inhibitors, RCAN1 overexpression in embryonic DRG neurons prolonged the APD_{90} (23.4% longer than control; $p = 0.037$) and slowed the maximum rate of repolarization (83.9% of control; $p = 0.033$). These changes are consistent with previously reported effects of Kv3.4 siRNA on the AP of DRG neurons (Ritter et al., 2012) and could be the result of optimizing the attenuation of the Kv3.4 current in embryonic DRG neurons (Fig. 11). In addition, as observed with CaN inhibitors (Table 1), RCAN1 overexpression decreased AP amplitude modestly (control: 100.02 ± 1.94 mV, RCAN1: 92.15 ± 2.32 mV, $p = 0.011$) and slowed the maximum rate of depolarization (control: 59.97 ± 4.82 ms/mV, RCAN1: 44.27 ± 3.78 ms/mV, $p = 0.014$).

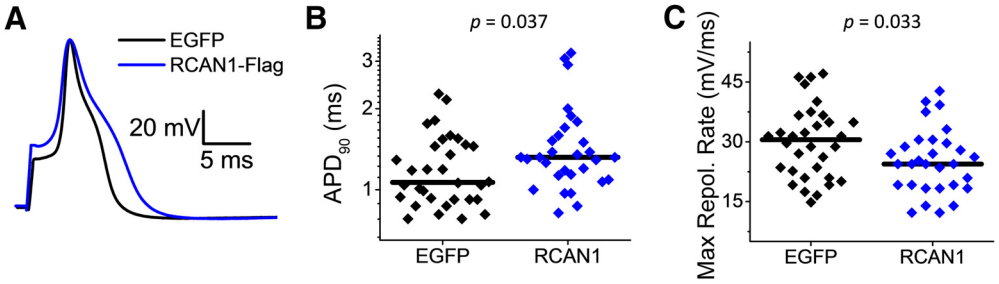

Figure 12. RCAN1 overexpression in embryonic DRG neurons prolongs the AP and slows the maximum rate of repolarization. ***A***, APs from DRG neurons transfected with EGFP + control plasmid (black) or EGFP + RCAN1-Flag containing plasmid (blue). ***B***, Comparison of the APD_{90} from control neurons (EGFP expressing, $n = 32$) and neurons overexpressing RCAN1-Flag ($n = 30$); p and median (bars) values are indicated in the graph (Wilcoxon–Mann–Whitney, $U = 331.5$). ***C***, Comparison of the maximum rate of repolarization from control neurons (EGFP expressing, $n = 32$) and neurons overexpressing RCAN1-Flag ($n = 30$); p and mean (bars) values are indicated in the graph (one-way ANOVA, DF = 1, $F = 4.78$). The diameters of the DRG neurons included here were (mean ± SEM): 20.9 ± 0.53 μm (controls) and 19.9 ± 0.5 μm (RCAN1).

Discussion

The ionic and molecular bases of peripheral mechanisms of SCI-induced persistent pain remain poorly understood. We have proposed previously that dysfunction of the Kv3.4 channel is a major determining factor of DRG hyperexcitability and the resulting persistent pathological pain in a rat model of cervical SCI (Ritter et al., 2015a, b). In a search for the signaling molecules and the mechanism responsible for SCI-induced Kv3.4 dysfunction, we investigated CaN, which has been implicated previously in pain syndromes associated with immunosuppressants and peripheral nerve lesions (Grotz et al., 2001; Miletic et al., 2002; Prommer, 2012; Miletic et al., 2015). The results demonstrate the following: (1) exposure of small-diameter DRG neurons to distinct CaN inhibitors prolongs the AP and decreases the maximum AP repolarization rate; (2) similar treatments induce attenuation of the Kv3.4 current and disrupt the current's fast inactivation profile in DRG neurons and a heterologous expression system; (3) attenuation of both peak currents and inactivation is eliminated by mutating NTID serines to alanine; (4) SCI induces Kv3.4 current alterations that mimic the effects of CaN inhibitors on this current; (5) SCI also induces upregulation of RCAN1 in DRG neurons, which has been shown to inhibit CaN activity; (6) overexpression of RCAN1 in naive DRG neurons is sufficient to induce Kv3.4 current alterations with features that recapitulate the effects of CaN inhibitors; and (7) overexpression of RCAN1 in naive DRG neurons is also sufficient to prolong the AP and slow the maximum AP repolarization rate. Altogether, these observations suggest that CaN is a key player in the phosphorylation-dependent modulation of the Kv3.4 channel NTID, which is dysregulated upon SCI. Moreover, novel SCI-induced RCAN1 upregulation in the DRG could be the primary alteration that drives Kv3.4 dysfunction and its effects on pain signaling.

Novel role of NTID phosphorylation sites on the modulation of Kv3.4 functional expression by CaN

PKC activation eliminates Kv3.4 fast N-type inactivation and, consequently, it initially increases the peak current (Covarrubias et al., 1994). The underlying mechanism of this modulation involving phosphorylation of four NTID serines is well established (Covarrubias et al., 1994; Beck et al., 1998; Antz et al., 1999) and it is not limited to heterologous expression systems. It exists in small-diameter DRG neurons, where it helps to shape the repolarization phase of the action potential (Ritter et al., 2012) and thus may regulate excitatory synaptic transmission in nociceptive areas of the spinal cord dorsal horn. Showing that CaN inhibition also disrupts fast Kv3.4 inactivation in this study has two major implications. First, it suggests that PKC and CaN represent the kinase and phosphatase that determine the phosphorylation status of the Kv3.4 NTID. Second, it suggests the presence of basal PKC activity and that the role of CaN under basal conditions is to maintain the NTID of Kv3.4 mostly dephosphorylated. Therefore, the Kv3.4 current would remain the fast inactivating A-type. Here, we determined a link between phosphorylation-dependent elimination of fast Kv3.4 inactivation and Kv3.4 current attenuation induced by CaN inhibitors. If PKC is activated further under conditions that favor NTID phosphorylation (i.e., CaN inhibition), then the Kv3.4 current would exhibit time-dependent modulation in two phases. During the early phase, the peak Kv3.4 current increases due to elimination of fast inactivation and persistent phosphorylation during a second late phase would induce slow current attenuation. Elucidating a mechanism, we discovered that the PKC phosphorylation sites within the NTID (S8, S9, S15, and S21) are also involved in the late attenuation of the Kv3.4 current induced by CaN inhibition. Such a novel role suggests that phosphorylation of the NTID might additionally modulate functional surface expression (trafficking and protein stability) and/or conductance. Although more complex scenarios are possible (e.g., involving ancillary subunits), the consistency of the electrophysiological effects with various CaN inhibitors in DRG neurons and confirmation of the modulations in a heterologous system help to establish CaN as a major modulator of the expression and function of the Kv3.4 channel through its effects on phosphorylation sites in the NTID.

In an alternate scenario, slowing of inactivation could have resulted from a Kv3.4-independent, CaN inhibitor-induced, delayed rectifier current. To test this possibility directly, we examined DRG neurons treated with Kv3.4 siRNA. Transfection of E18 DRG neurons with Kv3.4 siRNA nearly abolished the Kv3.4 current and treating these neurons with 1 μM FK506 induced no novel slow inactivating current. Therefore, in addition to current attenuation, CaN inhibition also induces the slowing of Kv3.4 inactivation as explained above.

Novel role of RCAN1 in maladaptive modulations induced by SCI in the DRG

SCI also induces simultaneous disruption of inactivation and current attenuation of the Kv3.4 current in small-diameter DRG neurons, which prompted us to investigate a possible role of CaN downregulation in the pathophysiology of SCI. However, we found that the expression of CaN Aα throughout the DRG was not downregulated by SCI. Instead, we discovered that the regu-

latory protein RCAN1 is upregulated in the cervical DRGs from SCI rats at both the mRNA and protein levels. RCAN1 is an essential endogenous regulator of CaN that is highly expressed in mammalian excitable tissues and inhibits CaN activity through a direct interaction (Hoeffer et al., 2007; Liu et al., 2009; Li et al., 2011; Shin et al., 2011). This inhibitory action is typically associated with upregulation or overexpression of RCAN1. Several studies have observed inhibition of NFAT translocation to the nucleus after RCAN1 upregulation, which confirms its negative impact on CaN activity (Davies et al., 2007; Liu et al., 2009; Li et al., 2011). In light of the available RCAN1 literature and our discovery, it is remarkable that overexpression of RCAN1 in DRG neurons is sufficient to induce a robust dual modulation of Kv3.4 channels that closely recapitulates the effects of pharmacological CaN inhibitors (in DRG neurons and CHO cells) and the effects of SCI. Therefore, given that SCI induces RCAN1 upregulation in DRG neurons, we can conclude that RCAN1 is a significant novel player in the pathophysiology of SCI. Through inhibition of CaN, RCAN1 upregulation might then ultimately be responsible for the attenuation of the Kv3.4 current with disrupted inactivation in small-diameter DRG neurons. Our previous work revealed that such a negative effect can be a major contributing factor to the hyperexcitability of small-diameter DRG neurons that is a basis of neuropathic pain induced by SCI (Ritter et al., 2015a). A recent study reported RCAN1 upregulation in the spinal cord dorsal horn after SCI (Wang et al., 2016). However, it was not clear whether the reported upregulation occurred in spinal neurons or synaptic terminals from primary sensory inputs in the dorsal horn. In addition, this study did not investigate the effects of RCAN1 upregulation on molecular targets that could alter neuronal excitability. Nevertheless, it supports independently a significant role of RCAN1 in the pathophysiology of SCI.

Pharmacological inhibition of CaN broadens the AP and slows its maximal rate of repolarization in DRG neurons, resembling the effects of Kv3.4 siRNA (Ritter et al., 2012). However, we found that overexpression of RCAN1 in adult neurons does not produce these effects. Rather, the effects of RCAN1-Flag overexpression resemble previously reported effects of SCI on Kv3.4 currents and DRG APs. We found that AP shape remained unchanged after SCI upon partial inhibition of the Kv3.4 current accompanied by slowing of inactivation (Ritter et al., 2015a). Contrary to what is normally observed under naive conditions, there was no AP shortening in response to PKC activation because, after incomplete attenuation, the remaining Kv3.4 current after SCI is already slow inactivating and cannot undergo further modulation of inactivation by PKC (Ritter et al., 2015a). Therefore, the magnitude of Kv3.4 current attenuation might ultimately determine whether there is broadening of the AP. Supporting this explanation, we found that optimized overexpression of RCAN1 in embryonic DRG neurons not only produces very robust attenuation of the Kv3.4 current exhibiting disrupted inactivation, it also prolongs the AP and slows the maximum rate of repolarization. Nucleofection of embryonic DRG neurons resulted in an 87% increase in RCAN1 expression, which is significantly greater than a more modest increase induced by SCI (27%). We do not know whether the SCI-induced RCAN1 upregulation alone is sufficient to generate the observed SCI-induced alterations in the Kv3.4 current and whether other factors are also involved. Most likely, SCI, like other injuries, induces multiple changes that could also affect Kv3.4 function. For instance, other pain injury models suggest changes that implicate PKCs in the DRG and spinal cord (Malmberg et al., 1997; Hucho and Levine, 2007). In our current working model, we propose that concerted PKC activation and CaN inhibition (with the latter resulting from RCAN1 upregulation) might lead to the level of Kv3.4 phosphorylation responsible for the observed changes after SCI. This is a likely scenario because promoting CaN inhibition experimentally upon RCAN1 overexpression alone seems able to match the SCI-induced Kv3.4 phosphorylation status, which could be responsible for the functional alterations. A possible contribution of novel factors, however, remains open.

Additional effects of CaN inhibition in the DRG

In addition to prolonging the AP and slowing its maximum repolarization rate, we found that CaN inhibition (induced by inhibitors or RCAN1 overexpression) decreased the AP amplitude modestly and slowed the maximum depolarization rate (Table 1). Decreased AP amplitude might negatively affect high-voltage-activating Kv channels, which could also contribute to broadening of the AP upon CaN inhibition. However, these effects are not observed upon knocking down Kv3.4 in DRG neurons with siRNA, as we reported previously (Ritter et al., 2012). Therefore, we suggest that CaN might additionally modulate voltage-gated Na^+ channels, a possibility that is not surprising given the widespread roles of CaN in excitable and nonexcitable tissues (Yakel, 1997; Rusnak and Mertz, 2000; Li et al., 2011).

Concluding remarks

The cellular and molecular bases of intractable pain in SCI and CIPS patients are poorly understood. The Kv3.4 channel is a key regulator of AP repolarization in putative DRG nociceptors. Here, we identified Kv3.4, CaN, and RCAN1 as key players in a putative peripheral mechanism of pain sensitization involving novel dysregulation of CaN signaling in DRG neurons. In particular, the results strongly suggest that RCAN1 is implicated in this mechanism through its downstream effects on the modulation of the Kv3.4 channel by CaN. In addition, we discovered that Kv3.4 NTID phosphorylation sites that modulate inactivation are involved in a novel mechanism that modulates Kv3.4 functional expression. These findings suggest tantalizing novel interventions to treat intractable pain more effectively in SCI and CIPS patients.

References

Ahn HS, Kim SE, Choi BH, Choi JS, Kim MJ, Rhie DJ, Yoon SH, Jo YH, Kim MS, Sung KW, Kwon OJ, Hahn SJ (2007) Calcineurin-independent inhibition of KV1. 3 by FK-506 (tacrolimus): a novel pharmacological property. Am J Physiol Cell Physiol 292:C1714–C1722. Medline

Antz C, Bauer T, Kalbacher H, Frank R, Covarrubias M, Kalbitzer HR, Ruppersberg JP, Baukrowitz T, Fakler B (1999) Control of K+ channel gating by protein phosphorylation: structural switches of the inactivation gate. Nat Struct Mol Biol 6:146–150. CrossRef Medline

Azzi JR, Sayegh MH, Mallat SG (2013) Calcineurin inhibitors: 40 years later, can't live without…. J Immunol 191:5785–5791. CrossRef Medline

Beck EJ, Sorensen RG, Slater SJ, Covarrubias M (1998) Interactions between multiple phosphorylation sites in the inactivation particle of a K+ channel insights into the molecular mechanism of protein kinase C action. J Gen Physiol 112:71–84. CrossRef Medline

Bedi SS, Yang Q, Crook RJ, Du J, Wu Z, Fishman HM, Grill RJ, Carlton SM, Walters ET (2010) Chronic spontaneous activity generated in the somata of primary nociceptors is associated with pain-related behavior after spinal cord injury. J Neurosci 30:14870–14882. CrossRef Medline

Chien LY, Cheng JK, Chu D, Cheng CF, Tsaur ML (2007) Reduced expression of A-type potassium channels in primary sensory neurons induces mechanical hypersensitivity. J Neurosci 27:9855–9865. CrossRef Medline

Cho KO, Kim YS, Cho YJ, Kim SY (2008) Upregulation of DSCR1 (RCAN1 or Adapt78) in the peri-infarct cortex after experimental stroke. Exp Neurol 212:85–92. CrossRef Medline

Covarrubias M, Wei A, Salkoff L, Vyas TB (1994) Elimination of rapid po-

tassium channel inactivation by phosphorylation of the inactivation gate. Neuron 13:1403–1412. CrossRef Medline

Davies KJ, et al. (2007) Renaming the DSCR1/Adapt78 gene family as RCAN: regulators of calcineurin. FASEB J 21:3023–3028. CrossRef Medline

Duan KZ, Xu Q, Zhang XM, Zhao ZQ, Mei YA, Zhang YQ (2012) Targeting A-type K+ channels in primary sensory neurons for bone cancer pain in a rat model. Pain 153:562–574. CrossRef Medline

Dubin AE, Patapoutian A (2010) Nociceptors: the sensors of the pain pathway. J Clin Invest 120:3760–3772. CrossRef Medline

Duprat F, Guillemare E, Romey G, Fink M, Lesage F, Lazdunski M, Honore E (1995) Susceptibility of cloned K+ channels to reactive oxygen species. Proc Natl Acad Sci U S A 92:11796–11800. CrossRef Medline

Fujii N, Ikeda K, Koyama M, Aoyama K, Masunari T, Kondo E, Matsuzaki T, Mizobuchi S, Hiraki A, Teshima T, Shinagawa K, Ishimaru F, Tanimoto M 2006) Calcineurin inhibitor-induced irreversible neuropathic pain after allogeneic hematopoietic stem cell transplantation. Int J Hematol 83: 459–461. CrossRef Medline

Gold MS, Gebhart GF (2010) Nociceptor sensitization in pain pathogenesis. Nat Med 16:1248–1257. CrossRef Medline

Goto S, Matsukado Y, Mihara Y, Inoue N, Miyamoto E (1986) The distribution of calcineurin in rat brain by light and electron microscopic immunohistochemistry and enzyme-immunoassay. Brain Res 397:161–172. CrossRef Medline

Grotz WH, Breitenfeldt MK, Braune SW, Allmann KH, Krause TM, Rump JA, Schollmeyer PJ (2001) Calcineurin-inhibitor induced pain syndrome (CIPS): a severe disabling complication after organ transplantation. Transpl Int 14:16–23. CrossRef Medline

Hashimoto Y, Perrino BA, Soderling TR (1990) Identification of an autoinhibitory domain in calcineurin. J Biol Chem 265:1924–1927. Medline

Hoeffer CA, Dey A, Sachan N, Wong H, Patterson RJ, Shelton JM, Richardson JA, Klann E, Rothermel BA (2007) The Down syndrome critical region protein RCAN1 regulates long-term potentiation and memory via inhibition of phosphatase signaling. J Neurosci 27:13161–13172. CrossRef Medline

Hucho T, Levine JD (2007) Signaling pathways in sensitization: toward a nociceptor cell biology. Neuron 55:365–376. CrossRef Medline

Hughes JP, et al. (2012) Understanding chronic inflammatory and neuropathic pain. Ann NY Acad Sci 1255:30–44. CrossRef Medline

Kipanyula MJ, Kimaro WH, Seke Etet PF (2016) The emerging roles of the calcineurin-nuclear factor of activated T-lymphocytes pathway in nervous system functions and diseases. J Aging Res 2016:5081021. CrossRef Medline

Lee S, Bang SM, Hong YK, Lee JH, Jeong H, Park SH, Liu QF, Lee IS, Cho KS (2016) The calcineurin inhibitor Sarah (Nebula) exacerbates Aβ42 phenotypes in a *Drosophila* model of Alzheimer's disease. DMM 9:295–306. CrossRef Medline

Li H, Rao A, Hogan PG (2011) Interaction of calcineurin with substrates and targeting proteins. Trends Cell Biol 21:91–103. CrossRef Medline

Liu J, Farmer JD Jr, Lane WS, Friedman J, Weissman I, Schreiber SL (1991) Calcineurin is a common target of cyclophilin-cyclosporin A and FKBP-FK506 complexes. Cell 66:807–815. CrossRef Medline

Liu Q, Busby JC, Molkentin JD (2009) Interaction between TAK1-TAB1-TAB2 and RCAN1-calcineurin defines a signalling nodal control point. Nat Cell Biol 11:154–161. CrossRef Medline

Li N, Lu ZY, Yu LH, Burnstock G, Deng XM, Ma B (2014) Inhibition of G-protein-coupled P2Y 2 receptor induced analgesia in a rat model of trigeminal neuropathic pain. Mol Pain 10:21. CrossRef Medline

Malmberg AB, Chen C, Tonegawa S, Basbaum AI (1997) Preserved acute pain and reduced neuropathic pain in mice lacking PKCγ. Science 278: 279–283. CrossRef Medline

Miletic G, Pankratz MT, Miletic V (2002) Increases in the phosphorylation of cyclic AMP response element binding protein (CREB) and decreases in the content of calcineurin accompany thermal hyperalgesia following chronic constriction injury in rats. Pain 99:493–500. CrossRef Medline

Miletic G, Sullivan KM, Dodson AM, Lippitt JA, Schneider JA, Miletic V (2011) Changes in calcineurin message, enzyme activity and protein content in the spinal dorsal horn are associated with chronic constriction injury of the rat sciatic nerve. Neuroscience 188:142–147. CrossRef Medline

Miletic G, Lippitt JA, Sullivan KM, Miletic V (2013) Loss of calcineurin in the spinal dorsal horn contributes to neuropathic pain, and intrathecal administration of the phosphatase provides prolonged analgesia. Pain 154:2024–2033. CrossRef Medline

Miletic G, Hermes JL, Bosscher GL, Meier BM, Miletic V (2015) Protein kinase C gamma-mediated phosphorylation of GluA1 in the postsynaptic density of spinal dorsal horn neurons accompanies neuropathic pain, and dephosphorylation by calcineurin is associated with prolonged analgesia. Pain 156:2514–2520. CrossRef Medline

Nicaise C, Hala TJ, Frank DM, Parker JL, Authelet M, Leroy K, Brion JP, Wright MC, Lepore AC (2012) Phrenic motor neuron degeneration compromises phrenic axonal circuitry and diaphragm activity in a unilateral cervical contusion model of spinal cord injury. Exp Neurol 235:539–552. CrossRef Medline

Noda Y, Kodama K, Yasuda T, Takahashi S (2008) Calcineurin-inhibitor-induced pain syndrome after bone marrow transplantation. J Anesth 22: 61–63. CrossRef Medline

Patel A, Yamashita N, Ascaño M, Bodmer D, Boehm E, Bodkin-Clarke C, Ryu YK, Kuruvilla R (2015) RCAN1 links impaired neurotrophin trafficking to aberrant development of the sympathetic nervous system in Down syndrome. Nat Commun 6:10119. CrossRef Medline

Prommer E (2012) Calcineurin-inhibitor pain syndrome. Clin J Pain 28: 556–559. CrossRef Medline

Richter A, Davies DE, Alexander P (1995) Growth inhibitory effects of FK506 and cyclosporin A independent of inhibition of calcineurin. Biochem Pharmacol 49:367–373. CrossRef Medline

Ritter DM, Ho C, O'Leary ME, Covarrubias M (2012) Modulation of Kv3. 4 channel N-type inactivation by protein kinase C shapes the action potential in dorsal root ganglion neurons. J Physiol 590:145–161. CrossRef Medline

Ritter DM, Zemel BM, Hala TJ, O'Leary ME, Lepore AC, Covarrubias M (2015a) Dysregulation of Kv3. 4 channels in dorsal root ganglia following spinal cord injury. J Neurosci 35:1260–1273. CrossRef Medline

Ritter DM, Zemel BM, Lepore AC, Covarrubias M (2015b) Kv3. 4 channel function and dysfunction in nociceptors. Channels 9:209–217. CrossRef Medline

Ruppersberg JP, Stocker M, Pongs O, Heinemann SH, Frank R, Koenen M (1991) Regulation of fast inactivation of cloned mammalian IK (A) channels by cysteine oxidation. Nature 352:711–714. CrossRef Medline

Rusnak F, Mertz P (2000) Calcineurin: form and function. Physiol Rev 80: 1483–1521. Medline

Sachewsky N, Hunt J, Cooke MJ, Azimi A, Zarin T, Miu C, Shoichet MS, Morshead CM (2014) Cyclosporin A enhances neural precursor cell survival in mice through a calcineurin-independent pathway. DMM 7:953–961. CrossRef Medline

Shin SY, Yang HW, Kim JR, Heo WD, Cho KH (2011) A hidden incoherent switch regulates RCAN1 in the calcineurin-NFAT signaling network. J Cell Sci 124:82–90. CrossRef Medline

Strack S, Wadzinski BE, Ebner FF (1996) Localization of the calcium/calmodulin-dependent protein phosphatase, calcineurin, in the hindbrain and spinal cord of the rat. J Comp Neurol 375:66–76. CrossRef Medline

Trimmer JS (2014) Ion channels and pain: Important steps towards validating a new therapeutic target for neuropathic pain. Exper Neurol 254:190. CrossRef Medline

Tsantoulas C, McMahon SB (2014) Opening paths to novel analgesics: the role of potassium channels in chronic pain. Trends Neurosci 37:146–158. CrossRef Medline

Walters ET (2012) Nociceptors as chronic drivers of pain and hyperreflexia after spinal cord injury: an adaptive-maladaptive hyperfunctional state hypothesis. Front Physiol 3:309.

Wang G, Zhao Y, Liu S, Jia J, Lu T (2016) Critical role of regulator of calcineurin 1 in spinal cord injury. J Physiol Biochem 72:605–613. CrossRef Medline

Yakel JL (1997) Calcineurin regulation of synaptic function: from ion channels to transmitter release and gene transcription. Trends Pharmacol Sci 18:124–134. Medline

Yang Q, Wu Z, Hadden JK, Odem MA, Zuo Y, Crook RJ, Frost JA, Walters ET (2014) Persistent pain after spinal cord injury is maintained by primary afferent activity. J Neurosci 34:10765–10769. CrossRef Medline